

Effective Warping Properties and Buckling Analysis of Fiber-Reinforced Elastomeric Isolators

Eduardo J. Montalto¹ and Dimitrios Konstantinidis²

¹Ph.D Candidate, Dept. of Civil and Environmental Engineering, Univ. of California, Berkeley,
CA 94720. Email: eduardo_montalto@berkeley.edu

²Associate Professor, Dept. of Civil and Environmental Engineering, Univ. of California,
Berkeley, CA 94720 (corresponding author). Email: konstantinidis@berkeley.edu

Abstract

Fiber-reinforced elastomeric isolators (FREIs) have been proposed as a cost-effective solution for expanding the use of seismic isolation to normal-importance structures. By using lightweight fiber reinforcement and eliminating the attachment plates, FREIs reduce cost while improving the isolation efficiency and reducing tensile stresses in the rubber. However, the flexural flexibility of the fiber allows cross-sectional distortions (i.e., warping) to occur, which significantly impacts the stability of these devices. This paper evaluates the buckling of rectangular, circular and annular FREIs, taking into account shear warping effects. A planar buckling theory previously proposed by the authors is adapted for the three-dimensional problem, and effective warping rigidities and warping-related areas are derived for the above bearing geometries, accounting for rubber compressibility. To assess the adequacy of the proposed buckling theory and derived warping properties in predicting the buckling of FREIs, a parametric finite element study is conducted. The critical load predictions of the proposed analytical formulation are found to be in excellent agreement with those of the numerical simulations. It is shown that traditional estimations of the buckling load that neglect warping are significantly unconservative. Finally, design recommendations and resources are provided for practice-oriented applications.

Keywords: Shear warping; Warping rigidity; Buckling theory; Fiber reinforced elastomeric isolators (FREIs); Stability of elastomeric bearings; Seismic isolation

INTRODUCTION

Elastomeric isolators consisting of thin rubber layers interleaved by reinforcement layers are vulnerable to buckling under compressive loads due to their high flexibility in shear. Haringx's buckling theory (1949), originally developed for helical springs and solid rubber rods, was adopted by Gent (1964) to study the buckling of thin rubber blocks bonded to steel plates, and has now become widely accepted to evaluate the stability of traditional steel-reinforced elastomeric isolators (SREIs) (Kelly and Konstantinidis 2011). Haringx's buckling load is given by:

$$P_{cr}^H = \frac{-P_S + \sqrt{P_S^2 + 4P_S P_E}}{2} \quad (1)$$

where $P_S = GA$ = the shear rigidity, $P_E = \pi^2 EI/h^2$ = Euler's critical load, and EI = the bending rigidity. In the context of SREIs, GA_b and \widetilde{EI}_b should be used instead, where $GA_b = GA(h/t_r)$ = the shear rigidity of the multilayer bearing, $\widetilde{EI}_b = \widetilde{EI}(h/t_r)$ = the *effective* bending rigidity of the multilayer bearing, \widetilde{EI} = the *effective* bending rigidity of a single rubber layer, h = total height of the bearing, and t_r = total height of rubber. Haringx's buckling load is derived from a one-dimensional beam theory which assumes that cross-sectional planes remain plane after deformation, but not orthogonal to the deformed axis, therefore allowing for shear deformations. This is suitable for SREIs where the steel plates are thick and very rigid in bending, and thus prevent cross-sectional distortions. However, this is not the case when the reinforcement is flexible in bending, as in the case of fiber-reinforced elastomeric isolators (FREIs), and cross-sectional warping due to transverse shear (i.e., shear warping) needs to be accounted for.

The first study concerning the buckling behavior of planar elastomeric bearings accounting for the impact of reinforcement flexural flexibility is by Simo (1982). Later, Kelly (1994) introduced an alternative formulation, which was later extended by Tsai and Kelly (2005a, 2005b). Both formulations, despite yielding significantly different results, predicted an important reduction in P_{cr}

48 with respect to Haringx's buckling load estimate. Recently, the stability of short beams accounting
49 for shear warping has been revisited in (Montalto and Konstantinidis, "Buckling of short beams",
50 submitted, *J. Eng. Mech.*, ASCE). A buckling formulation was derived from the consistent lin-
51 earization of a fully geometrically nonlinear planar beam accounting for warping where the finite
52 deformation field was posed as that of a constrained director Cosserat rod. The resulting theory
53 generalizes the one by Kelly and Tsai, and accounts for warping effects as well as axial shorten-
54 ing of the element. Its applicability to FREIs was verified using a parametric finite element study
55 of infinite strip isolators, where the predictions of the analytical formulation were shown to be
56 in excellent agreement with results from the numerical simulations. This study also provided a
57 comparison with respect to previous buckling formulations that account for warping.

58 The buckling formulation presented in (Montalto and Konstantinidis, "Buckling of short beams",
59 submitted, *J. Eng. Mech.*, ASCE), as well as the earlier one by Kelly and Tsai, make use of an *ef-*
60 *fective* isolator warping rigidity and warping-related cross-sectional areas. These were derived for
61 an infinite strip bearing by Tsai and Kelly (2005a) accounting for fiber extensibility, and extended
62 in (Montalto and Konstantinidis, "Buckling of short beams", submitted, *J. Eng. Mech.*, ASCE)
63 to also consider rubber compressibility. Both of these results are based on the usual kinematic
64 assumptions of a parabolic bulging shape and linear variation of displacements through the thick-
65 ness of the rubber layer, and the assumption that normal stresses in the rubber are dominated by
66 the pressure, leading to the so-called *pressure solution*. The warping properties of an infinite strip
67 bearing were also derived by Pinarbasi and Mengi (2008, 2017) using an approximate formulation
68 based on a modified Galerkin method which uses weighted averages of displacements and stresses
69 through the layer thickness, and does not depend on the assumptions cited before; reinforcement
70 flexibility and rubber compressibility were considered. Despite recognition of the significant effect
71 of warping on the mechanical response of FREIs since their inception (Kelly 1999), warping for
72 bearing geometries other than infinite strip has been unexplored thus far (Van Engelen 2019).

73 The present study investigates the warping response of three-dimensional FREIs and the im-
74 pact of warping on their stability under compressive loads. First, the buckling theory presented

75 in (Montalto and Konstantinidis, "Buckling of short beams", submitted, *J. Eng. Mech.*, ASCE) is
76 revisited, and the necessary modifications to apply it to three-dimensional elements are described.
77 In particular, warping distortions vary depending on the cross-sectional geometry of the element,
78 and thus a specific warping function for each geometry is proposed. Then, the effective warping
79 rigidity and warping-related cross-sectional areas are derived for rectangular, circular and annular
80 bearings following the assumptions of the pressure solution. Rubber compressibility is accounted
81 for, but fiber extensibility is neglected based on results from previous studies on planar infinite strip
82 bearings which indicate negligible impact of this parameter on their warping properties and sta-
83 bility (Pinarbasi and Mengi 2008, 2017; Montalto and Konstantinidis, "Buckling of short beams",
84 submitted, *J. Eng. Mech.*, ASCE). The use of the cited buckling theory together with the derived
85 warping properties is evaluated on the basis of a three-dimensional parametric finite element study
86 for unbonded FREIs. Recommendations for the estimation of the buckling of FREIs are given and
87 design resources are provided to aid the practical implementation of these results.

88 **BUCKLING THEORY**

89 **Planar Formulation**

90 The buckling of a planar beam accounting for nonuniform shear warping and axial shortening was
91 presented in (Montalto and Konstantinidis, "Buckling of short beams", submitted, *J. Eng. Mech.*,
92 ASCE). The beam with reference configuration $\mathcal{B} \subset \mathbb{R}^2$ such that $\mathcal{B} = \mathcal{A} \times [0, h]$, with cross section
93 $\mathcal{A} \subset \mathbb{R}$ and height $h \in \mathbb{R}$ is assumed to lie in the xz plane such that its line of centroids is aligned
94 with the z axis in the undeformed configuration (see Fig. 1). Then, the beam deforms according to
95 the displacement field \mathbf{u} with x and z components given by:

$$u_x = v(z) \quad u_z = \Delta(z) - x\psi(z) - f_w(x)\phi(z) \quad (2)$$

96 where $\Delta(z)$, $v(z)$ = the vertical and lateral displacements of the beam's axis, respectively, $\psi(z)$ =
97 the cross-sectional rotation in the absence of warping, and $\phi(z)$ = the dimensionless amplitude
98 multiplier for the cross-sectional warping $f_w(x)$.

99 The following conditions are enforced to decouple the generalized stress resultants P (axial
100 load), M (bending moment), and Q (warping moment):

$$\int_{\mathcal{A}} f_w \sigma_{\Delta}(x) dA = 0 \quad \int_{\mathcal{A}} f_w \sigma_{\psi}(x) dA = 0 \quad \int_{\mathcal{A}} \sigma_{\phi}(x) dA = 0 \quad \int_{\mathcal{A}} x \sigma_{\phi}(x) dA = 0 \quad (3)$$

101 where $\sigma_{\Delta}(x)$, $\sigma_{\psi}(x)$, $\sigma_{\phi}(x)$ = the axial stresses caused by an axial displacement, a rotation, and a
102 warping deformation, respectively. These conditions impose restrictions on the definitions of the
103 warping function $f_w(x)$. In the case of a homogeneous isotropic beam, such restrictions are:

$$\int_{\mathcal{A}} f_w(x) dA = 0 \quad \int_{\mathcal{A}} x f_w(x) dA = 0 \quad (4)$$

104 which allow the interpretation of $\Delta(z)$ and $v(z)$ as the average axial and transverse displacements,
105 respectively, and of $\psi(z)$ as the average rotation of the cross section.

106 Based on the previous displacement field and the assumption that stresses normal and tangent to
107 the cross section are linear with respect to their work-conjugate strains, the following second-order
108 accurate potential can be established for the beam:

$$\Pi(v, \psi, \phi) = \frac{1}{2} \int_0^h \begin{Bmatrix} \psi' \\ \phi' \\ \tilde{\gamma} \\ \tilde{\phi} \end{Bmatrix}^T \begin{pmatrix} EI & 0 & 0 & 0 \\ 0 & EJ & 0 & 0 \\ 0 & 0 & GA + \tilde{P} & -GB - \tilde{P} \frac{f_B}{A} \\ 0 & 0 & -GB - \tilde{P} \frac{f_B}{A} & GC + \tilde{P} \frac{f_C}{A} \end{pmatrix} \begin{Bmatrix} \psi' \\ \phi' \\ \tilde{\gamma} \\ \tilde{\phi} \end{Bmatrix} - \tilde{P}(v')^2 dz \quad (5)$$

109 where $\tilde{\gamma} = v' - \lambda_o \psi$, $\tilde{\phi} = \lambda_o \phi$, $\tilde{P} = P/\lambda_o$, and $\lambda_o = 1 - P/EA$ = the initial stretch of the beam due
110 to the application of the axial load P . Moreover, EA , GA and EI correspond to the axial, shear and
111 bending rigidities as normally defined, while EJ , B , C , f_B and f_C are the effective warping rigidity
112 and warping-related areas dependent on the definition of the function f_w .

113 The equilibrium equations, shown in (Montalto and Konstantinidis, "Buckling of short beams",
114 submitted, *J. Eng. Mech.*, ASCE), can be obtained by virtue of the principle of virtual work such
115 that $\delta\Pi = 0$. These equations along with the appropriate boundary conditions are then used to

116 obtain the critical load for the element. For a beam with fixed end conditions (i.e, no rotation or
 117 warping at the supports) but free to sway at the top, the normalized critical load $\bar{P}_{cr} = P_{cr}/GA$
 118 corresponds to the solution of the following quartic equation:

$$\bar{P} \left\{ \left[\bar{P} + \lambda_o(\bar{P}) \right] \kappa_C(\bar{P}) - \lambda_o(\bar{P}) \kappa_B(\bar{P}) \right\} + \pi^2 \Omega \left\{ \bar{P} \left[\bar{P} + \lambda_o(\bar{P}) \right] + \kappa_B(\bar{P}) - \kappa_C(\bar{P}) \right\} - \pi^4 \Omega^2 = 0 \quad (6)$$

119 where $\Omega = EI/GAh^2$ is the bending-to-shear stiffness ratio, while $\lambda_o(\bar{P})$, $\kappa_B(\bar{P})$ and $\kappa_C(\bar{P})$ are:

$$\lambda_o(\bar{P}) = 1 - \bar{P} \frac{GA}{EA} \quad (7)$$

$$\kappa_B(\bar{P}) = \left(\bar{P} \frac{f_B}{A} + \lambda_o \frac{B}{A} \right)^2 \frac{EI}{EJ} \quad \kappa_C(\bar{P}) = \lambda_o \left(\bar{P} \frac{f_C}{A} + \lambda_o \frac{C}{A} \right) \frac{EI}{EJ} \quad (8)$$

121 Hereinafter, Eq. (6) will be referred to as the *proposed-exact* equation.

122 Alternatively, the buckling load can be calculated from the approximate equation:

$$P_{cr} \approx \sqrt{\frac{P_S P_E}{1 + \left(\frac{f_B}{A} \right)^2 \frac{EI}{EJ}}} \quad (9)$$

123 where $P_S = GA =$ shear rigidity, and $P_E = \pi^2 EI/h^2 =$ Euler's buckling load. Haringx's buckling
 124 load [Eq. (1)] can be approximated by $P_{cr}^H \approx \sqrt{P_S P_E}$ when $P_E \gg P_S$. Then, Eq. (9) can be
 125 interpreted as this critical load reduced on the basis of the bending-to-warping rigidity ratio EI/EJ
 126 and the ratio f_B/A , which measures the angular deviation of the line of action of the axial load
 127 P with respect to the normal to the average cross-sectional plane. Eq. (9) was shown to predict
 128 critical loads very close to those of Eq. (6) for infinite strip bearings (Montalto and Konstantinidis,
 129 "Buckling of short beams", submitted, *J. Eng. Mech.*, ASCE). In the following, Eq. (9) will be
 130 referred to as the *proposed-approximate* equation.

131 **Extension to Three-Dimensional Case**

132 In the three-dimensional case, the beam has a cross section $\mathcal{A} \subset \mathbb{R}^2$, assumed to be doubly-
 133 symmetrical, such that its reference configuration $\mathcal{B} \subset \mathbb{R}^3$ is defined as $\mathcal{B} = \mathcal{A} \times [0, h]$. In the

134 undeformed configuration, the cross section lies in the xy plane such that x and y correspond to the
135 symmetry axis, while z is the centroidal axis as before. The lateral deformation is still assumed
136 to occur in the xz plane, and the interpretation of the generalized displacements Δ , ν , ψ and ϕ
137 and the cross-sectional warping f_w remains the same. Again, the cross-sectional warping function
138 satisfies the orthogonality conditions in Eq. (3) [or Eq. (4) for the homogeneous isotropic case].
139 The only difference is that f_w is now, in general, a function of both x and y . The definition of this
140 cross-sectional warping function for a two-dimensional cross section is detailed next.

141 *Warping function*

142 In three-dimensional beam theories that consider cross-sectional warping (developed for numerical
143 implementation), the warping function has often been taken as that from the solution to Saint-
144 Venant's flexure problem with vanishing Poisson's ratio ν (El Fatmi 2007; Genoese et al. 2013;
145 Dikaros and Sapountzakis 2014; Lewiński and Czarnecki 2021). This leads to formulations that
146 account for out-of-plane cross-sectional warping but neglect in-plane cross-sectional distortion.
147 In this study, this approach is adopted and the warping function is based on the so-called Saint-
148 Venant warping. However, the latter function needs to be further modified to allow the axial load,
149 the bending moment and the warping moment to be decoupled for the stress distribution that occurs
150 in the bearings, which differs from that of homogeneous isotropic beams.

151 The Saint-Venant flexure problem consists of determining the three-dimensional linear elas-
152 ticity solution to the problem of a cantilever beam subjected to tractions at its free end which are
153 statically equivalent to a transverse load H acting through the centroid of the cross section. At the
154 fixed end of the beam the centroidal displacement and a rotation are imposed to be zero, but no fur-
155 ther essential boundary conditions are imposed. The traction boundary conditions at the free-end
156 are specified in terms of the resultant transverse load H , while the point-wise tractions are assumed
157 to be applied in such a way that they coincide with the stress distribution from the solution. Hence,
158 this solution corresponds to that of unrestrained warping and end-effects are neglected. The prob-
159 lem has been solved in classic texts [e.g., Love (1944)] in terms of displacements for common
160 cross-sectional geometries, including rectangular and circular ones.

161 The Saint-Venant warping function $f_w^{SV}(x, y)$ can be extracted from the exact displacement so-
 162 lutions presented, for example, by Love (1944) as shown in (Cowper 1966; Simo 1982). However,
 163 under the assumption of $\nu = 0$, a simpler approach can be adopted as illustrated next. The three-
 164 dimensional beam $\mathcal{B} \subset \mathbb{R}^3$ is defined as before with a height h and a cross section $\mathcal{A} \subset \mathbb{R}^2$ with
 165 boundary $\partial\mathcal{A}$ and normal vector \mathbf{v} , such that $\mathcal{B} = \mathcal{A} \times [0, h]$. In the undeformed configuration,
 166 the cross section lies in the xy plane, while the line of centroids of the beam is aligned with the z
 167 axis. The semi-fixed end is taken at $z = 0$, while tractions are applied at $z = h$ with a resultant H
 168 acting in the x direction through the centroid of the cross section. The cross-sectional boundary is
 169 traction-free throughout the beam such that $\boldsymbol{\sigma}\mathbf{v} = \mathbf{0}$ on $\partial\mathcal{A}$.

170 The exact displacement field for Saint-Venant's flexure problem with vanishing Poisson's ratio
 171 can be expressed as:

$$u_x = v(z) \quad u_y = 0 \quad u_z = -x\psi(z) - f_w^{SV}(x, y)[v'(z) - \psi(z)] \quad (10)$$

172 plus a rigid-body motion which depends on the specific rotation boundary condition enforced at the
 173 semi-fixed end $z = 0$. In this case, $v(z)$ and $\psi(z)$ have the same interpretation as before, being the
 174 average transverse displacement and average cross-sectional rotation respectively, while $f_w^{SV}(x, y)$
 175 satisfies the orthogonality conditions in Eq. (4).

176 Defining the function $\Phi(x, y)$ as:

$$\Phi(x, y) = x - f_w^{SV}(x, y) \quad (11)$$

177 the strains can be written as:

$$\varepsilon_z = -\psi'x - f_w^{SV}(v'' - \psi') \quad \gamma_{xz} = \Phi_{,x}(v' - \psi) \quad \gamma_{yz} = \Phi_{,y}(v' - \psi) \quad (12)$$

178 with the rest of the strains being equal to zero; the notation $(\bullet)_{,x}$ represents the partial deriva-
 179 tive with respect to x . For a homogeneous isotropic material with Young's modulus E and shear

180 modulus G , the stresses are given by:

$$\sigma_z = -E[\psi'x + f_w^{SV}(v'' - \psi')] \quad \tau_{xz} = G\Phi_{,x}(v' - \psi) \quad \tau_{yz} = G\Phi_{,y}(v' - \psi) \quad (13)$$

181 Moreover, the traction-free boundary condition for the cross section now reads $\nabla\Phi \cdot \mathbf{v} = 0$ on $\partial\mathcal{A}$.

182 Neglecting body forces, the equations from the balance of linear momentum corresponding to
 183 $\text{div}(\boldsymbol{\sigma}) \cdot \mathbf{e}_x = 0$ and $\text{div}(\boldsymbol{\sigma}) \cdot \mathbf{e}_y = 0$ result in $(v'' - \psi') = 0$. Multiplying the last equilibrium equation
 184 $\text{div}(\boldsymbol{\sigma}) \cdot \mathbf{e}_z = 0$ by x , integrating over the cross section and making use of $\boldsymbol{\sigma}\mathbf{v} = \mathbf{0}$ on $\partial\mathcal{A}$, the
 185 relation $-EI\psi'' = \kappa GA(v' - \psi)$ is recovered, where κ has been defined as:

$$\kappa = \frac{\int_{\mathcal{A}} \Phi_{,x} dA}{A} \quad (14)$$

186 Using this relation in $\text{div}(\boldsymbol{\sigma}) \cdot \mathbf{e}_z = 0$, the following is obtained:

$$\nabla^2\Phi + \frac{\kappa A}{I}x = 0 \quad (15)$$

187 The Saint-Venant warping function can be determined by solving the elliptic problem in Eq.
 188 (15) over the cross section \mathcal{A} , with the traction boundary condition $\nabla\Phi \cdot \mathbf{v} = 0$ on $\partial\mathcal{A}$ and the
 189 relation $f_w^{SV} = x - \Phi$. Additionally, the orthogonality conditions in Eq. (4) need to be enforced
 190 to uniquely define the solution. Following this approach, the Saint-Venant warping function is
 191 obtained for a rectangular cross section with width $2b$ in the x direction and depth $2l$ in the y
 192 direction:

$$f_w^{SV}(x, y) = \frac{5}{6} \left(\frac{x^3}{2b^2} - \frac{3}{10}x \right) \quad (16)$$

193 For the circular and annular cross sections, we make use of polar coordinates such that $x = r \cos(\theta)$
 194 and $y = r \sin(\theta)$. Then, the warping function for these cross sections is given by:

$$f_w^{SV}(r, \theta) = \frac{\kappa}{1 + \eta^2} \left[\frac{r^3}{2b^2} + \left(\frac{1}{\kappa} - \frac{3}{2} \right) (1 + \eta^2)r - \frac{3\eta^2 b^2}{2r} \right] \cos(\theta), \quad \kappa = \frac{6(1 + \eta^2)^2}{7 + 34\eta^2 + 7\eta^4} \quad (17)$$

195 where b = the exterior radius of the cross section, a = the interior radius, and $\eta = a/b$ = the
 196 interior-to-exterior radius ratio; for a circular cross section $\eta = 0$.

197 Enforcing the orthogonality conditions in Eq. (4) allows to decouple the generalized stress
 198 resultants P , M and Q in the case of an isotropic homogeneous beam. However, for an elastomeric
 199 bearing the stress distributions are not proportional to the cross-sectional deformations, and thus
 200 the general conditions in Eq. (3) are required. The Saint-Venant warping functions are then modi-
 201 fied to allow the satisfaction of these requirements. For the rectangular case we use:

$$f_w(x, y) = \frac{5}{6} \left(\frac{x^3}{2b^2} + \omega x \right) \quad (18)$$

202 For the circular and annular cross sections we have:

$$f_w(r, \theta) = \frac{6}{7} \left(\frac{r^3}{2b^2} + \omega r - \frac{3\eta^2 b^2}{2r} \right) \cos(\theta) \quad (19)$$

203 where ω is a parameter that depends on the cross section and material properties, which is obtained
 204 from the satisfaction of Eq. (3). These warping functions are shown in Fig. 2.

205 **EFFECTIVE WARPING PROPERTIES**

206 Whereas the buckling theory assumes a homogeneous isotropic material in the element, the me-
 207 chanical response of an elastomeric isolator is governed by the composite action of the rubber
 208 and the reinforcement, producing different stress distributions than those obtained by the beam
 209 theory. *Effective* rigidities are thus required to apply the buckling theory to elastomeric isolators;
 210 see discussion following Eq. (1) for the analogous case of using Haringx's theory for SREIs. The
 211 effective axial and bending rigidities, \widetilde{EA} and \widetilde{EI} , considering rubber compressibility but not rein-
 212 forcement extensibility have already been presented for different bearing geometries by Kelly and
 213 Konstantinidis (2011). In the following, the effective warping-related properties for bearings with
 214 rectangular, circular and annular cross section are derived.

Boundary Value Problem

The effective rigidities are obtained by evaluating the mechanical response of a single rubber layer of thickness t_e using linear elasticity and following traditional assumptions regarding the deformation of the layer and the stress distribution (Kelly and Konstantinidis 2011). Namely, it is assumed that vertical lines are deformed into a parabola, and that the vertical displacement varies linearly throughout the layer. Furthermore, it is assumed that the normal stresses are dominated by the internal pressure p such that $\sigma_x \approx \sigma_y \approx \sigma_z \approx -p$, while the in-plane shear stress $\tau_{xy} \approx 0$. This leads to the so-called *pressure solution* (Gent and Lindley 1959; Gent and Meinecke 1970; Kelly and Konstantinidis 2011). These assumptions have been shown to be accurate for layers of nearly incompressible material bonded to nearly inextensible reinforcement when the shape factors S (i.e., ratio of loaded to force-free area) are in the typical range used in elastomeric isolators (10 - 30) using more refined analytical solutions (Papoulia and Kelly 1996; Pinarbasi and Mengi 2008).

Pinarbasi and Mengi (2008, 2017) showed that, for layers of nearly incompressible material with high shape factor bonded to reinforcement with axial rigidity values characteristic of the fiber in FREIs, reinforcement extensibility has a negligible influence on the effective warping rigidity of infinite strip bearings. Moreover, results in (Montalto and Konstantinidis, "Buckling of short beams", submitted, *J. Eng. Mech.*, ASCE) indicated that reinforcement extensibility has a negligible effect in the buckling of planar infinite strip bearings considering realistic material parameters and thickness of the fiber. Reinforcement extensibility is measured by the dimensionless parameter $\alpha \propto \sqrt{Gt_e/E_f t_f} S$, where E_f = fiber Young's modulus, and t_f = fiber thickness, while rubber compressibility is measured by the dimensionless parameter $\beta \propto \sqrt{G/K} S$, where K = rubber bulk modulus (Van Engelen et al. 2016). For a given shape factor S , the required thickness t_e of a three-dimensional layer is smaller than that of its planar counterpart. Thus, α is reduced while β remains the same and the influence of fiber extensibility is expected to be even lower in three-dimensional bearings. Therefore, the following analysis will account for rubber compressibility but neglect the extensibility of the fiber reinforcement.

Following the presentation for the beam theory, it is assumed that the isolator's axis is oriented

242 along the z direction with the mid-height of the layer located at $z = 0$, while the reinforcement lies
 243 in the xy plane (see Fig. 3). Then, the assumed displacement field is as follows:

$$u(\mathbf{x}) = u_0(x, y) \left(1 - \frac{4z^2}{t_e^2}\right) \quad v(\mathbf{x}) = v_0(x, y) \left(1 - \frac{4z^2}{t_e^2}\right) \quad w(\mathbf{x}) = -f_w(x, y) \phi \frac{z}{t_e} \quad (20)$$

244 where $u(\mathbf{x})$, $v(\mathbf{x})$ and $w(\mathbf{x})$ are the displacement fields in the x , y and z directions respectively, and
 245 $u_0(x, y)$ and $v_0(x, y)$ are functions to be determined based on the solution to the boundary-value
 246 problem. As indicated before, it is assumed that the displacement along the axis of the beam varies
 247 linearly. Hence, $\phi/2$ corresponds to the warping amplitude at the top and bottom of the layer, while
 248 the term z/t_e provides the linear variation of the displacement explicitly. The warping function
 249 $f_w(x, y)$ depends on the cross-sectional geometry and is given by Eq. (18) for the rectangular case,
 250 and Eq. (19) for the circular and annular ones. The corresponding strain fields for the rubber are:

$$\varepsilon_x(\mathbf{x}) = u_{0,x} \left(1 - \frac{4z^2}{t_e^2}\right) \quad \varepsilon_y(\mathbf{x}) = v_{0,y} \left(1 - \frac{4z^2}{t_e^2}\right) \quad \varepsilon_z(\mathbf{x}) = -f_w \frac{\phi}{t_e} \quad (21)$$

$$\gamma_{xz}(\mathbf{x}) = -\left(\frac{8u_0}{t_e} + f_{w,x}\phi\right) \frac{z}{t_e} \quad \gamma_{yz}(\mathbf{x}) = -\left(\frac{8v_0}{t_e} + f_{w,y}\phi\right) \frac{z}{t_e} \quad (22)$$

251 The material constitutive relation for the volumetric deformation of the rubber is given by
 252 $\text{tr}(\boldsymbol{\varepsilon}) = -p(x, y)/K$, where K = bulk modulus of the rubber, leading to the equation:
 253

$$(u_{0,x} + v_{0,y}) \left(1 - \frac{4z^2}{t_e^2}\right) - f_w \frac{\phi}{t_e} = -\frac{p}{K} \quad (23)$$

254 Integrating this equation through the thickness of the rubber layer, we obtain:

$$\frac{2}{3} (u_{0,x} + v_{0,y}) - f_w \frac{\phi}{t_e} = -\frac{p}{K} \quad (24)$$

255 The shear stresses are obtained from the material constitutive relation:

$$\tau_{xz}(\mathbf{x}) = -G \left(\frac{8u_0}{t_e} + f_{w,x}\phi\right) \frac{z}{t_e} \quad \tau_{yz}(\mathbf{x}) = -G \left(\frac{8v_0}{t_e} + f_{w,y}\phi\right) \frac{z}{t_e} \quad (25)$$

256 where G = shear modulus of the rubber.

257 Now we make use of the balance of linear momentum for the rubber layer, which in the absence
258 of body forces and under quasi-static conditions reads $\text{div}(\boldsymbol{\sigma}) = \mathbf{0}$. Under the assumptions that the
259 normal stresses are dominated by the pressure and that τ_{xy} is negligible in comparison to the other
260 stress components, the first equation of equilibrium, corresponding to $\text{div}(\boldsymbol{\sigma}) \cdot \mathbf{e}_x = 0$, results in:

$$p_{,x} + \frac{G}{t_e} \left(\frac{8u_0}{t_e} + f_{w,x}\phi \right) = 0 \quad (26)$$

261 The second equilibrium equation, corresponding to $\text{div}(\boldsymbol{\sigma}) \cdot \mathbf{e}_y = 0$, becomes:

$$p_{,y} + \frac{G}{t_e} \left(\frac{8v_0}{t_e} + f_{w,y}\phi \right) = 0 \quad (27)$$

262 Taking the partial derivative of Eq. (26) with respect to x , the partial derivative of Eq. (27)
263 with respect to y , adding them together, and substituting $u_{0,x} + v_{0,y}$ using Eq. (24), we obtain the
264 following equation for the pressure $p(x, y)$:

$$\nabla^2 p - \left(\frac{12G}{Kt_e^2} \right) p = -\frac{12G\phi}{t_e^3} \left(f_w + \frac{t_e^2}{12} \nabla^2 f_w \right) \quad (28)$$

265 For rubber layers with a shape factor S in the range used for elastomeric isolators (10-30), the last
266 term in the parenthesis of the right-hand side of the pressure equation is at least a couple of orders
267 of magnitude smaller than the leading terms and is thus neglected in the following.

268 The pressure distribution on the layer due to a warping deformation is obtained from Eq. (28),
269 alongside the boundary condition $p = 0$ on the cross-sectional boundary. This pressure distribution
270 is then used to determine the effective warping rigidity and warping-related areas, following their
271 definitions given in (Montalto and Konstantinidis, "Buckling of short beams", submitted, *J. Eng.*
272 *Mech.*, ASCE), recalling that the warping displacement has been assumed to vary linearly in the

273 rubber layer such that $\phi' = \phi/t_e$ and taking $P/A = (\Delta/t_e)(\widetilde{EA}/A)$:

$$\widetilde{EJ} = \frac{\int_{\mathcal{A}} f_w p dA}{\phi/t_e} \quad (29)$$

$$274 \quad B = \int_{\mathcal{A}} f_{w,x} dA \quad C = \int_{\mathcal{A}} (f_{w,x})^2 dA \quad (30)$$

$$275 \quad f_B = \frac{A \int_{\mathcal{A}} f_{w,x} p_{\Delta} dA}{(\Delta/t_e) \widetilde{EA}} \quad f_C = \frac{A \int_{\mathcal{A}} (f_{w,x})^2 p_{\Delta} dA}{(\Delta/t_e) \widetilde{EA}} \quad (31)$$

276 where p_{Δ} = pressure due to an axial shortening displacement Δ , and \widetilde{EA} = effective axial rigidity.

277 **Rectangular Layer**

278 For the case of a rectangular cross section, we consider the layer to have a width of $2b$ in the x
279 direction and a depth of $2l$ in the y direction. Therefore, the shape factor is given by:

$$S = \frac{bl}{(b+l)t_e} = \frac{b}{t_e} \frac{1}{(1+\rho)} \quad (32)$$

280 where $\rho = b/l$ gives the in-plane aspect ratio of the bearing. Making use of the warping function
281 in Eq. (18), the partial differential equation for the pressure can be restated as:

$$p_{,xx} + p_{,yy} - \left(\frac{\beta}{b}\right)^2 p = -\frac{10G\phi}{t_e^3} \left(\frac{x^3}{2b^2} + \omega x\right) \quad (33)$$

282 where,

$$\beta^2 = \frac{12Gb^2}{Kt_e^2} = \frac{12G}{K} S^2 (1+\rho)^2 \quad (34)$$

283 The solution to Eq. (33) is obtained by assuming a single Fourier series in the x direction. The
284 resulting pressure is given by:

$$p(x, y) = 10GS^2(1+\rho)^2 \left(\frac{b\phi}{t_e}\right) \sum_{n=1}^{\infty} \frac{(-1)^n [6 - n^2\pi^2(1+2\omega)]}{\xi_n^2 n^3 \pi^3} \left[1 - \frac{\cosh(\xi_n y/b)}{\cosh(\xi_n/\rho)}\right] \sin\left(\frac{n\pi x}{b}\right) \quad (35)$$

285 where $\xi_n^2 = (n\pi)^2 + \beta^2$. The parameter ω is obtained using Eq. (3). Albeit not shown here for

286 brevity, the first two conditions are analogous to the third and fourth conditions, and the latter two
 287 are used. The third condition is trivially satisfied. The fourth condition yields:

$$\sum_{n=1}^{\infty} \frac{n^2 \pi^2 (1 + 2\omega) - 6}{n^4 \pi^4 \xi_n^2} \left[1 - \frac{\tanh(\xi_n/\rho)}{\xi_n/\rho} \right] = 0 \quad (36)$$

288 Because the pressure in the rectangular layer is given in terms of an infinite Fourier series, the
 289 orthogonality condition for the warping function does not have a closed-form solution for ω ; hence
 290 Eq. (36) requires to be solved numerically. In general, it depends on the ratio K/G , the in-plane
 291 aspect ratio ρ and the shape factor S . Numerical results for this are presented in Fig. 4.

292 The effective warping rigidity \widetilde{EJ} and the cross-sectional areas B and C can then be obtained
 293 from their definitions in Eqs. (29) and (30):

$$\widetilde{EJ} = \frac{50 GS^2 (1 + \rho)^2 b^4}{3 \rho} \sum_{n=1}^{\infty} \frac{[n^2 \pi^2 (1 + 2\omega) - 6]^2}{n^6 \pi^6 \xi_n^2} \left[1 - \frac{\tanh(\xi_n/\rho)}{\xi_n/\rho} \right] \quad (37)$$

$$B = \frac{5b^2}{3\rho} (1 + 2\omega) \quad (38)$$

$$C = \frac{5b^2}{36\rho} (9 + 20\omega + 20\omega^2) \quad (39)$$

296 For the calculation of the areas f_B and f_C , the pressure due to a vertical displacement Δ , denoted
 297 p_Δ , is required. This has been presented by Kelly and Konstantinidis (2011) accounting for rubber
 298 compressibility. When the origin of the Cartesian system is located at the centroid of the layer, this
 299 pressure is given by:

$$p_\Delta(x, y) = 48GS^2(1 + \rho)^2 \left(\frac{\Delta}{t_e} \right) \sum_{n=1}^{\infty} \frac{(-1)^n}{\zeta_n^2 (2n - 1)\pi} \left[1 - \frac{\cosh(\zeta_n y/b)}{\cosh(\zeta_n/\rho)} \right] \cos \left[\frac{(2n - 1)\pi x}{2b} \right] \quad (40)$$

300 where $\zeta_n^2 = [(2n - 1)\pi/2]^2 + \beta^2$. The effective axial rigidity \widetilde{EA} is given by:

$$\widetilde{EA} = \frac{384GS^2(1 + \rho)^2 b^2}{\rho} \sum_{n=1}^{\infty} \frac{1}{\zeta_n^2 (1 - 2n)^2 \pi^2} \left[1 - \frac{\tanh(\zeta_n/\rho)}{\zeta_n/\rho} \right] \quad (41)$$

301 Using Eq. (31), the areas f_B and f_C are given by:

$$f_B = \frac{5b^2 \sum_{n=1}^{\infty} \frac{[-24+(1-2n)^2\pi^2(3+2\omega)] \left\{1 - \frac{\tanh(\zeta_n/\rho)}{\zeta_n/\rho}\right\}}{\zeta_n^2(1-2n)^4\pi^4}}{3\rho \sum_{n=1}^{\infty} \frac{1}{\zeta_n^2(1-2n)^2\pi^2} \left\{1 - \frac{\tanh(\zeta_n/\rho)}{\zeta_n/\rho}\right\}} \quad (42)$$

$$f_C = \frac{25b^2 \sum_{n=1}^{\infty} \frac{[3456+(1-2n)^4\pi^4(3+2\omega)^2-48(1-2n)^2\pi^2(9+2\omega)] \left\{1 - \frac{\tanh(\zeta_n/\rho)}{\zeta_n/\rho}\right\}}{\zeta_n^2(1-2n)^6\pi^6}}{36\rho \sum_{n=1}^{\infty} \frac{1}{\zeta_n^2(1-2n)^2\pi^2} \left\{1 - \frac{\tanh(\zeta_n/\rho)}{\zeta_n/\rho}\right\}} \quad (43)$$

302
303 The previous results provide all the warping related properties needed for the estimation of the
304 buckling load. However, the effective bending rigidity \widetilde{EI} is also required. Accounting for rubber
305 compressibility, this is given by (Kelly and Konstantinidis 2011):

$$\widetilde{EI} = \frac{96GS^2(1+\rho)^2b^4}{\rho} \sum_{n=1}^{\infty} \frac{1}{n^2\pi^2\xi_n^2} \left[1 - \frac{\tanh(\xi_n/\rho)}{\xi_n/\rho}\right] \quad (44)$$

306 The critical load for the bearing can then be computed using Eqs. (6) or (9) with the previous
307 effective cross-sectional properties. Fig. 5 presents the comparison between the critical load esti-
308 mates of these equations as a function of the shape factor S and the width-to-height aspect ratio
309 $S_2^* = 2b/h$. These results verify that the proposed-approximate solution [Eq. (9)] provides close
310 estimates to those of Eq. (6) for the isolator with rectangular cross section.

311 Circular and Annular Layers

312 For the circular and annular cases, we consider the layer to have an exterior radius of b , an
313 interior radius a , and an interior-to-exterior radius ratio $\eta = a/b$; for circular cross sections $\eta = 0$.
314 Hence, the shape factor is given by:

$$S = \frac{b-a}{2t_e} = \frac{b(1-\eta)}{2t_e} \quad (45)$$

315 In this case the warping function is given by Eq. (19). Then, the partial differential equation for
 316 the pressure [Eq. (28)] in polar coordinates becomes:

$$p_{,rr} + \frac{1}{r}p_{,r} + \frac{1}{r^2}p_{,\theta\theta} - \left(\frac{\beta}{b}\right)^2 p = -\frac{72G\phi}{7t_e^3} \left(\frac{r^3}{2b^2} + \omega r - \frac{3\eta^2 b^2}{2r} \right) \cos(\theta) \quad (46)$$

317 where the non-dimensional ratio β measuring the compressibility of the material corresponds to:

$$\beta^2 = \frac{12Gb^2}{Kt_e^2} = \frac{48GS^2}{K(1-\eta)^2} \quad (47)$$

318 *Circular Layer*

319 For the circular layer, the solution to Eq. (46) is given in terms of modified Bessel functions of the
 320 first kind of order m , referenced as $I_m(r)$:

$$p(r, \theta) = \frac{144GS^2}{7\beta^2} \left(\frac{b\phi}{t_e} \right) \left\{ \left(\frac{r}{b} \right)^3 + 2 \left(\frac{r}{b} \right) \left(\frac{4}{\beta^2} + \omega \right) - \frac{[1 + 2(4/\beta^2 + \omega)]I_1(\beta r/b)}{I_1(\beta)} \right\} \cos(\theta) \quad (48)$$

321 As before, the parameter ω defining the warping function $f_w(r, \theta)$ is calculated from satisfying the
 322 third and fourth orthogonality conditions in Eq. (3) (equivalent to the first two conditions). The
 323 third orthogonality condition is directly satisfied. Then, the fourth orthogonality condition is used
 324 to determine ω , and the following is obtained:

$$\omega = \frac{-\beta(12 + \beta^2)I_1(\beta) + 6(8 + \beta^2)I_2(\beta)}{3\beta^3 I_3(\beta)} \quad (49)$$

325 The warping properties are then obtained following the same approach as for the rectangular
 326 layer. Using Eq. (29), the effective warping rigidity is given by:

$$\widetilde{EJ} = \frac{18\pi GS^2 b^4}{49\beta^2} \left\{ 3 + 8\omega(2 + 3\omega) + \frac{16(5 + 12\omega)}{\beta^2} + \frac{384}{\beta^4} - \frac{24[8 + \beta^2(1 + 2\omega)]^2 I_2(\beta)}{\beta^5 I_1(\beta)} \right\} \quad (50)$$

327 The areas B and C are calculated from Eq. (30):

$$B = \frac{3}{7}\pi b^2(1 + 2\omega) \quad (51)$$

328

$$C = \frac{9}{98}\pi b^2(3 + 8\omega + 8\omega^2) \quad (52)$$

329 The calculation of the areas f_B and f_C requires the pressure p_Δ . When accounting for rubber
330 compressibility, this corresponds to (Kelly and Konstantinidis 2011):

$$p_\Delta(r, \theta) = \frac{48GS^2}{\beta^2} \left(\frac{\Delta}{t} \right) \left[1 - \frac{I_0(\beta r/b)}{I_0(\beta)} \right] \quad (53)$$

331 The effective axial rigidity \widetilde{EA} for the circular cross section is:

$$\widetilde{EA} = \frac{48\pi GS^2 b^2}{\beta^2} \frac{I_2(\beta)}{I_0(\beta)} \quad (54)$$

332 Hence, the areas f_B and f_C [Eq. (31)] are given by:

$$f_B = \frac{3}{7}\pi b^2 \left\{ \frac{\beta[8 + \beta^2(1 + 2\omega)]I_0(\beta) - 4[4 + \beta^2(1 + \omega)]I_1(\beta)}{\beta^3 I_2(\beta)} \right\} \quad (55)$$

333

$$f_C = \frac{9}{98}\pi b^2 \left\{ \frac{\beta\{576 + 8\beta^2(9 + 8\omega) + \beta^4[3 + 8\omega(1 + \omega)]\}I_0(\beta)}{\beta^5 I_2(\beta)} \right. \quad (56)$$

$$\left. - \frac{2\{576 + 16\beta^2(9 + 4\omega) + \beta^4[9 + 8\omega(2 + \omega)]\}I_1(\beta)}{\beta^5 I_2(\beta)} \right\}$$

334 Similar to the case of the rectangular bearings, it is convenient to provide the effective bending
335 rigidity, which corresponds to (Kelly and Konstantinidis 2011):

$$\widetilde{EI} = \frac{48\pi b^4 GS^2}{\beta^2} \left[\frac{1}{4} - \frac{I_2(\beta)}{\beta I_1(\beta)} \right] \quad (57)$$

336 Then, the critical load for the bearing can be computed using the proposed-exact expression [Eq.

337 (6)] or the proposed-approximate closed-form solution [Eq. (9)] with the effective cross-sectional
338 properties presented before. Fig. 6 shows that Eq. (9) provides excellent agreement with Eq. (6)
339 for the circular bearing. In this figure results are presented in terms of the shape factor S and the
340 width-to-height aspect ratio $S_2^* = 2b/h$.

341 *Annular Layer*

342 Albeit common in the context of SREIs, annular FREIs have seldom been explored. Only recently
343 have they been evaluated with the purpose of isolating lightweight structures and nonstructural
344 components (Ghorbi and Toopchi-Nezhad 2023). Because of this and the length and complexity
345 of the resulting equations, the corresponding effective warping rigidity and warping-related cross-
346 sectional properties are presented in Appendix I for the interested reader. Using these properties,
347 Fig. 6 shows the excellent agreement between Eqs. (6) and (9) for the critical load estimation of
348 annular bearings.

349 Kelly and Konstantinidis (2011) recognized that, when warping is neglected, the introduction
350 of an inner hole in the bearing causes a negligible reduction in the critical pressure $p_{cr} = P_{cr}/A$,
351 and the reduction in the critical load is approximately of the same proportion as the area reduction.
352 However, this is not the case when warping occurs, as illustrated in Fig. 7, where the critical
353 pressure of an annular bearing has been normalized by that of a circular bearing with the same
354 outer radius and layer thickness. When neglecting warping, an inner hole with $\eta = 0.40$ reduces
355 p_{cr} by no more than 15%, while the reduction for smaller holes is negligible. In contrast, when
356 accounting for warping using Eq. (6) and the properties in Appendix I, even a small hole with $\eta =$
357 0.1 reduces p_{cr} as much as 35%, while for $\eta = 0.4$ this reduction is greater than 70% in some cases.
358 Note that the critical load P_{cr} is reduced even further due to the area reduction.

359 **FINITE ELEMENT ANALYSIS**

360 The use of the proposed effective warping properties and Eq. (9) was validated by a finite ele-
361 ment parametric study developed using the nonlinear FEA software Marc (Hexagon AB 2021a).
362 Isolators with rectangular, circular and annular cross sections were modeled in an unbonded con-
363 figuration, and the critical load estimates from the numerical models were used as a benchmark to

364 evaluate the analytical formulation. In the following, the modeling and results are described.

365 **Modeling**

366 To avoid volumetric locking and element failure due to mesh distortions, mixed-formulation low-
 367 order elements were used for the rubber. A three-field formulation proposed by Simo et al. (1985)
 368 was used; it is derived from a variational principle using the following functional:

$$\Pi(\boldsymbol{\varphi}, p, \theta) = \int_{\mathcal{B}} [\hat{W}(\hat{\mathbf{C}}) + U(\theta) + p(J - \theta)] dV + \Pi_{ext}(\boldsymbol{\varphi}) \quad (58)$$

369 where the fields are $\boldsymbol{\varphi}$ = deformation, p = pressure, and θ = volumetric strain. Additionally,
 370 $J = \det(\mathbf{F})$, where $\mathbf{F} = \partial\boldsymbol{\varphi}/\partial\mathbf{X}$ = the deformation gradient, and $\Pi_{ext}(\boldsymbol{\varphi})$ = the external potential
 371 energy due to the imposed body forces and surface tractions; $\hat{W}(\hat{\mathbf{C}})$ and $U(\theta)$ are defined in the
 372 following. The functional $\Pi(\boldsymbol{\varphi}, p, \theta)$ uses the multiplicative split of \mathbf{F} given by:

$$\bar{\mathbf{F}} = \theta^{1/3} \hat{\mathbf{F}}, \quad (59)$$

373 where $\hat{\mathbf{F}} = J^{-1/3} \mathbf{F}$ = isochoric part of \mathbf{F} . The domains were discretized using Q1-P0 hexahe-
 374 dral elements, which use continuous piecewise trilinear interpolation for the deformation field and
 375 piecewise constant interpolation for the pressure and volumetric strain fields (Simo et al. 1985);
 376 this corresponds to element type 7 in Marc with the constant dilation parameter activated (Hexagon
 377 AB 2021b). They were implemented in an Updated Lagrangian formulation.

378 An additive split of the strain energy $W(\bar{\mathbf{C}}) = \hat{W}(\hat{\mathbf{C}}) + U(\theta)$ has been assumed in Eq. (58), where
 379 \hat{W} and U are the deviatoric and volumetric parts of the strain energy, respectively, and $\hat{\mathbf{C}} = \hat{\mathbf{F}}^T \hat{\mathbf{F}}$
 380 is the modified right Cauchy-Green deformation tensor. A compressible neo-Hookean model was
 381 used for the rubber, whose corresponding deviatoric strain energy defined by the shear modulus G
 382 and bulk modulus K is given by:

$$\hat{W}(\hat{\mathbf{C}}) = \frac{G}{2} (I_{\hat{\mathbf{C}}} - 3) \quad (60)$$

383 where $I_{\hat{\mathbf{C}}} = \text{tr}(\hat{\mathbf{C}})$. This model is considered to represent rubber response accurately in the small to

384 moderate deformation range (principal stretches in the range of 0.5-2.0) (Treloar 2005; Steigmann
385 2017), which covers the range of deformation exhibited in the numerical simulations. The follow-
386 ing volumetric strain energy satisfying polyconvexity and growth conditions was used:

$$U(\theta) = K \left(\frac{\theta^2 - 1}{4} - \frac{\ln \theta}{2} \right) \quad (61)$$

387 Only half of each isolator was modeled considering symmetry conditions (see Fig. 8); for the
388 nodes lying on the plane of symmetry, no displacement was allowed perpendicular to such plane.
389 Three elements were used along the height of each rubber layer. For the isolators with rectangular
390 cross section, a structured mesh was applied using transfinite interpolation such that a coarser
391 mesh with element width-to-height aspect ratios of approximately 4:1 was produced at the interior
392 of the bearing, and a finer mesh was produced towards the edges. In the case of the circular and
393 annular isolators, a two-dimensional unstructured mesh was produced over the cross section using
394 Marc's MoM mesh generator (Hexagon AB 2021a); this planar mesh was later extruded to produce a
395 structured mesh over the height of the bearing. In this case, the width-to-height aspect ratio of the
396 elements was maintained at 2:1 over the entire bearing. These mesh sizes were verified to achieve
397 convergence of the estimated critical loads.

398 The fiber reinforcement was modeled using quadrilateral membrane elements in a Total La-
399 grangian formulation; this corresponds to element type 18 in Marc (Hexagon AB 2021b). These
400 elements use bilinear displacement interpolation and have no flexural rigidity. Moreover, they
401 have zero out-of-plane thickness and therefore the overall height-to-total rubber thickness ratio
402 $h/t_r = 1$ in the models. The fiber reinforcement material is modeled as linear elastic, defined by
403 its Young's modulus E_f and Poisson's ratio ν_f . The contact between the bearing and its supports
404 and the bearing with itself was modeled with a node-to-segment formulation, where the top and
405 bottom supports were represented by rigid planar surfaces. Coulomb friction was used to model
406 the friction between isolator and its supports with a friction coefficient $\mu = 1$.

Buckling Analysis Method

The isolator model was progressively loaded by a compressive axial load P in the range of 0.5 to 1.5 times the critical load estimated by Eq. (9). After every ramp load increment of 5%, the axial load was held constant while a small lateral perturbation was applied to the model (see Fig. 9a). This perturbation corresponded to a maximum lateral displacement u_{x0} of 0.2 mm at the top support, inducing an average shear strain of 0.2% in the isolator. Based on this, the global lateral stiffness of the isolator K_h was measured at different axial loads. The buckling load was taken as the axial load at which K_h vanishes (see Fig. 9b).

Cases

The variable parameters in the study were the shape factor S , the width-to-height aspect ratio S_2^* , the in-plane aspect ratio ρ for rectangular isolators, and the interior-to-exterior radius ratio η for circular and annular isolators. The values for these parameters included in the analysis are presented in Table 1; the values presented for S_2^* are satisfied exactly, while reported S are target values and the actual values of the models differ slightly from those in Table 1. All the combinations between these parameters were considered, except those leading to less than 5 or more than 25 rubber layers which were deemed unrealistic for practical scenarios. Hence, a total of 100 cases were evaluated, 50 of which were bearings with rectangular cross section and the remaining ones with circular or annular cross section. In all the analyses the bearing height was fixed at 100 mm, the rubber was modeled with a shear modulus $G = 0.4$ MPa and bulk modulus $K = 2000$ MPa, while the fiber reinforcement was modeled with a fiber thickness $t_f = 0.5$ mm, Young's modulus $E_f = 100000$ MPa, and Poisson's ratio $\nu_f = 0.20$.

Results

The FEA results are used as a benchmark to study the adequacy of the buckling theory and the effective warping properties derived herein. Figs. 10 and 11 present the critical loads estimated with the proposed-approximate formulation [Eq. (9)] normalized by the critical loads from the FEA models. As can be interpreted from Figs. 5 and 6, the results for the proposed-exact formulation are nearly identical to those of Eq. (9), and hence are not presented in the following. Figures 10

434 and 11 also present the critical loads estimated using Haringx's theory for comparison purposes.
435 The estimates using the proposed-approximate equation and Haringx's theory have both used the
436 effective properties accounting for rubber compressibility, but not fiber extensibility.

437 Figures 10 and 11 show that the proposed-approximate formulation exhibits excellent agree-
438 ment with the results obtained from the FEA models. The critical loads tend to be slightly underes-
439 timated by the proposed formulation when the isolators have low shape factors S , associated with
440 higher compressibility. Similar findings were shown for the planar bearings in (Montalto and Kon-
441 stantinidis, "Buckling of short beams", submitted, *J. Eng. Mech.*, ASCE), where it was explained
442 how bearings with low S experience larger vertical deformation and lateral expansion before buck-
443 ling, leading to an increase in cross-sectional dimensions that increases their critical load; this is
444 not accounted for by the one-dimensional buckling formulation. However, the cross-sectional ex-
445 pansion in the three-dimensional isolators occurs in two-directions and thus has a less significant
446 effect in the results than for the planar infinite strip bearings. Therefore, the proposed-approximate
447 formulation presents a better performance for the three-dimensional bearings than the planar ones,
448 for which it was already satisfactory.

449 In contrast, Figs. 10 and 11 show that Haringx's theory can severely overestimate the buckling
450 load of FREIs. This overestimation was in the range of 1.35 - 2.0 times the critical load obtained
451 from the FEA models for rectangular isolators, and in the range of 1.35 - 1.75 for circular ones,
452 with the error increasing with the shape factor S . For annular bearings the overprediction is greater
453 and, for the cases evaluated, lies between 2.0 - 3.0 times the P_{cr} from the FEA models. The
454 error increases again with S but also increases significantly with the relative size of the inner hole
455 measured by η ; this is in agreement with results presented in Fig. 7. In the case of SREIs, the
456 introduction of an inner hole in a circular bearing has a negligible effect on its stability (Kelly and
457 Konstantinidis 2011). However, this is not the case for FREIs. Despite not being evaluated here, it
458 is expected that the introduction of a hole on rectangular FREIs would yield similar results. Interior
459 holes in FREIs have been proposed to reduce the isolator lateral stiffness for applications dealing
460 with lightweight structures (Van Engelen et al. 2014; Osgooei et al. 2015; Ghorbi and Toopchi-

461 [Nezhad 2023](#)). It is recognized that, despite the severe reduction in critical load, stability might
462 not be an issue in those cases. However, the impact of compressive loads on the lateral behavior
463 can be significant as the axial load will be much closer to the critical load than formerly expected.

464 **RECOMMENDATIONS FOR DESIGN**

465 Based on the results from the finite element analysis, the buckling theory presented in (Montalto
466 and Konstantinidis, "Buckling of short beams", submitted, *J. Eng. Mech.*, ASCE) along with the
467 effective warping properties derived herein produce an adequate estimation of the critical load for
468 FREIs. Therefore, it is recommended that either Eq. (6) or Eq. (9) be used to evaluate the stability
469 of FREIs. The latter, however, is deemed more useful for practical application purposes due to
470 its simplicity. Rubber compressibility should be accounted for in the calculation of the effective
471 rigidities, especially for bearings with moderate-to-high shape factor S . Alternatively, the buckling
472 load accounting for warping can be presented as:

$$P_{cr} = \frac{P_{cr}^H}{f_R} \quad (62)$$

473 where P_{cr}^H is the critical load due to Haringx's theory given by Eq. (1). This reduction factor has
474 been computed using Eq. (6) for different geometric and material parameters, and is presented in
475 Figs. 12 and 13 for practical implementation of these results.

476 It should be noted that $h/t_r = 1$ has been assumed thus far due to the negligible fiber thickness
477 t_f in comparison to the rubber thickness of a single layer t_e for typical FREIs. However, for some
478 bearing configurations with very thin rubber layers, this might not hold. For SREIs the approach
479 has been to increase the effective rigidities of a single layer (e.g., GA , \widetilde{EI} , \widetilde{EJ}) by the factor h/t_r
480 ([Gent 1964](#); [Kelly and Konstantinidis 2011](#)); see discussion following Eq. (1). Following this
481 approach, effective rigidities for the multilayer bearing [e.g., $\widetilde{EI}_b = \widetilde{EI}(h/t_r)$] should be used in
482 Eqs. (6) and (9). Alternatively, Eq. (9) shows that this simply leads to an amplification factor
483 of h/t_r for P_{cr} calculated using the effective rigidities of a single layer presented before, and this
484 approach is recommended due to the multiple effective properties required in Eqs. (6) or (9). The

485 detailed calculation of the effective warping properties and buckling load for each of the bearing
486 geometries presented in this study is illustrated in Appendix II.

487 **CONCLUSIONS**

488 This study investigated the warping of three-dimensional FREIs and its impact on their buckling
489 load P_{cr} . First, modifications necessary to apply the planar buckling theory accounting for shear
490 warping previously presented by the authors were described. In particular, warping functions were
491 introduced for each of the evaluated cross sections by modifying the warping displacements from
492 the Saint-Venant flexure problem to allow for decoupling of the generalized stress resultants in the
493 isolators. Then, effective warping properties were derived for rectangular, circular and annular iso-
494 lators, following the usual assumptions from the *pressure solution*. In these derivations, the effect
495 of rubber compressibility was included but fiber extensibility was neglected because previous stud-
496 ies noted the latter to have a negligible influence on the warping properties and stability of planar
497 FREIs. Using these properties, it was shown that the proposed-exact and proposed-approximate
498 equations for estimating the critical load are in excellent agreement for three-dimensional isolators.

499 The use of the proposed-approximate buckling formulation and the effective warping related
500 properties to predict the stability of FREIs was validated through a finite element parametric study
501 on the stability of rectangular, circular and annular FREIs. The results from the proposed analytical
502 formulation match closely the results from the numerical simulations for all examined bearing
503 geometries. Moreover, it was shown that neglecting warping effects by using Haringx's theory
504 can result in significantly unconservative estimates of P_{cr} for FREIs. Based on these findings,
505 it is recommended that warping effects be considered when evaluating the stability of FREIs by
506 using either the proposed exact or approximate buckling load equation in conjunction with the
507 effective warping properties derived herein. Alternatively, figures providing a reduction factor for
508 the buckling load with respect to Haringx's theory due to warping effects have been provided to
509 facilitate the practical application of these results. Furthermore, in contrast to the case of SREIs,
510 introducing a hole in FREIs was found to severely reduce their stability. Therefore, caution is
511 advised when introducing these modifications in the isolators.

512 **APPENDIX I. EFFECTIVE WARPING PROPERTIES FOR ANNULAR LAYER**

513 The pressure in an annular layer is obtained from solving Eq. (46) with the boundary conditions

514 $p(a, \theta) = p(b, \theta) = 0$. The pressure is given by:

$$p(r, \theta) = \frac{144GS^2}{7\beta^2(1-\eta)^2} \left(\frac{b\phi}{t_e} \right) \left\{ \left(\frac{r}{b} \right)^3 + 2 \left(\frac{r}{b} \right) \left(\frac{4}{\beta^2} + \omega \right) - 3\eta^2 \left(\frac{b}{r} \right) + D_1 I_1 \left(\frac{\beta r}{b} \right) + D_2 K_1 \left(\frac{\beta r}{b} \right) \right\} \cos(\theta) \quad (63)$$

515 where $I_m(r)$ and $K_m(r)$ are the modified Bessel functions of the 1st and 2nd kind of order m , and,

$$D_1 = \frac{\left[2 \left(\frac{1}{2} + \frac{4}{\beta^2} + \omega \right) - 3\eta^2 \right] K_1(\beta\eta) - \eta^3 \left[1 + \frac{2}{\eta^2} \left(\frac{4}{\beta^2} + \omega - \frac{3}{2} \right) \right] K_1(\beta)}{I_1(\beta\eta)K_1(\beta) - I_1(\beta)K_1(\beta\eta)} \quad (64)$$

$$D_2 = - \frac{\left[2 \left(\frac{1}{2} + \frac{4}{\beta^2} + \omega \right) - 3\eta^2 \right] I_1(\beta\eta) - \eta^3 \left[1 + \frac{2}{\eta^2} \left(\frac{4}{\beta^2} + \omega - \frac{3}{2} \right) \right] I_1(\beta)}{I_1(\beta\eta)K_1(\beta) - I_1(\beta)K_1(\beta\eta)}$$

516 Enforcing the third and fourth orthogonality conditions in Eq. (3) (and in passing satisfying the
517 first and second conditions), the parameter ω from the warping function is obtained:

$$\omega = \frac{W_1}{W_2} \quad (65)$$

518 where,

$$W_1 = 12\eta \left[\beta^2(1 + \eta^2) - 8 \right] + \beta \left\{ W_3 I_2(\beta\eta) K_1(\beta) + W_4 I_2(\beta) K_1(\beta\eta) \right. \\ \left. + I_1(\beta\eta) [W_4 K_2(\beta) - W_5 K_1(\beta)] + I_1(\beta) [W_3 K_2(\beta\eta) + W_5 K_1(\beta\eta)] \right\} \quad (66)$$

$$W_2 = 3\beta^2 \left\{ 8\eta + \beta \left[\beta I_3(\beta) K_1(\beta\eta) + I_1(\beta\eta) [\beta(\eta^4 - 1) K_1(\beta) - 4K_2(\beta)] \right. \right. \\ \left. \left. - \eta^3 [4I_2(\beta\eta) K_1(\beta) + \beta\eta I_1(\beta) K_3(\beta\eta)] \right] \right\}$$

519 and,

$$W_3 = 6\eta^3 [8 + \beta^2(\eta^2 - 3)]$$

$$W_4 = 6(8 + \beta^2 - 3\beta^2\eta^2) \quad (67)$$

$$W_5 = \beta(\eta^2 - 1) [12(1 + \eta^2) + \beta^2(1 - 8\eta^2 + \eta^4)]$$

520 Using Eq. (29) for the effective warping rigidity, and Eq. (30) for the areas B and C , these
 521 properties are calculated as:

$$\begin{aligned} \widetilde{EJ} = & \frac{108\pi GS^2 b^4}{49\beta^2(1-\eta)^2} \left\{ \left(\frac{1+2\omega}{\beta} + \frac{8}{\beta^3} \right) [D_1 I_2(\beta) - D_2 K_2(\beta)] - \frac{2}{\beta^2} [D_1 I_1(\beta) + D_2 K_1(\beta)] \right. \\ & - \left(\frac{\eta^4 + 2\omega\eta^2}{\beta} + \frac{8\eta^2}{\beta^3} \right) [D_1 I_2(\beta\eta) - D_2 K_2(\beta\eta)] + \frac{2\eta^3}{\beta^2} [D_1 I_1(\beta\eta) + D_2 K_1(\beta\eta)] \\ & - \frac{3\eta^2}{\beta} \left\{ D_1 [I_0(\beta) - I_0(\beta\eta)] - D_2 [K_0(\beta) - K_0(\beta\eta)] \right\} + \frac{1-\eta^8}{8} - 9\eta^4 \log(\eta) \\ & \left. + \left(\frac{4}{\beta^2} + 2\omega \right) \left[\frac{1-\eta^6}{3} + 3(\eta^4 - \eta^2) \right] + (1-\eta^4) \left[\omega \left(\frac{4}{\beta^2} + \omega \right) - \frac{3\eta^2}{2} \right] \right\} \end{aligned} \quad (68)$$

$$522 \quad B = \frac{3\pi}{7} b^2 (1-\eta^2)(1+\eta^2+2\omega) \quad (69)$$

$$523 \quad C = \frac{9\pi}{98} b^2 (1-\eta^2) [3 + 3\eta^4 + 8\omega(1+\omega) + 2\eta^2(9+4\omega)] \quad (70)$$

524 The pressure due to an axial displacement Δ , p_Δ , and the effective axial rigidity \widetilde{EA} have been
 525 presented by Kelly and Konstantinidis (2011) and are given by:

$$p_\Delta(r) = \frac{48GS^2}{\beta^2(1-\eta)^2} \left(\frac{\Delta}{t_e} \right) \left[1 + D_3 I_0 \left(\frac{\beta r}{b} \right) + D_4 K_0 \left(\frac{\beta r}{b} \right) \right] \quad (71)$$

$$526 \quad \widetilde{EA} = \frac{48\pi GS^2 b^2}{\beta^2(1-\eta)^2} \left\{ 1 - \eta^2 + \frac{2D_3}{\beta} [I_1(\beta) - \eta I_1(\beta\eta)] - \frac{2D_4}{\beta} [K_1(\beta) - \eta K_1(\beta\eta)] \right\} \quad (72)$$

527 where,

$$D_3 = \frac{K_0(\beta\eta) - K_0(\beta)}{I_0(\beta\eta)K_0(\beta) - I_0(\beta)K_0(\beta\eta)} \quad D_4 = -\frac{I_0(\beta\eta) - I_0(\beta)}{I_0(\beta\eta)K_0(\beta) - I_0(\beta)K_0(\beta\eta)} \quad (73)$$

528 Then, the effective warping areas f_B and f_C [Eq. (31)] correspond to:

$$f_B = \frac{12\pi}{7} \frac{\int_{\eta b}^b \left[\left(\frac{r}{b} \right)^2 + \omega \right] \left[1 + D_3 I_0 \left(\frac{\beta r}{b} \right) + D_4 K_0 \left(\frac{\beta r}{b} \right) \right] r dr}{\left\{ 1 - \eta^2 + \frac{2D_3}{\beta} [I_1(\beta) - \eta I_1(\beta\eta)] - \frac{2D_4}{\beta} [K_1(\beta) - \eta K_1(\beta\eta)] \right\} / (1-\eta^2)} \quad (74)$$

$$529 \quad f_C = \frac{9\pi}{49} \frac{\int_{\eta b}^b \left[9 \left(\frac{r}{b} \right)^4 + 16\omega \left(\frac{r}{b} \right)^2 + (8\omega^2 + 6\eta^2) + 9\eta^4 \left(\frac{b}{r} \right)^4 \right] \left[1 + D_3 I_0 \left(\frac{\beta r}{b} \right) + D_4 K_0 \left(\frac{\beta r}{b} \right) \right] r dr}{\left\{ 1 - \eta^2 + \frac{2D_3}{\beta} [I_1(\beta) - \eta I_1(\beta\eta)] - \frac{2D_4}{\beta} [K_1(\beta) - \eta K_1(\beta\eta)] \right\} / (1-\eta^2)} \quad (75)$$

530 The solution to the integral in Eq. (74), albeit available, is impractical due to its complexity, while
 531 the integral in Eq. (75) does not have a closed-form solution. Nevertheless, both integrals can be
 532 solved by numerical integration along the radial direction.

533 Lastly, the effective bending rigidity for annular bearings is provided for completeness. It
 534 corresponds to (Kelly and Konstantinidis 2011):

$$\widetilde{EI} = \frac{48\pi GS^2 b^4}{\beta^2(1-\eta)^2} \left\{ \frac{1-\eta^2}{4} + \frac{D_5}{\beta} [I_2(\beta) - \eta^2 I_2(\beta\eta)] - \frac{D_6}{\beta} [K_2(\beta) - \eta^2 K_2(\beta\eta)] \right\} \quad (76)$$

535 where,

$$D_5 = \frac{K_1(\beta\eta) - \eta K_1(\beta)}{I_1(\beta\eta)K_1(\beta) - I_1(\beta)K_1(\beta\eta)} \quad D_6 = -\frac{I_1(\beta\eta) - \eta I_1(\beta)}{I_1(\beta\eta)K_1(\beta) - I_1(\beta)K_1(\beta\eta)} \quad (77)$$

536 This provides all the effective properties required to use Eqs. (6) or (9) for annular FREIs.

537 APPENDIX II. EXAMPLE CALCULATIONS FOR VERIFICATION

538 In Table 2, results are presented for each of the effective rigidities and warping-related areas to
 539 allow users to verify the proper implementation of the equations; results for the buckling loads are
 540 also presented. Three-cases are analyzed: a rectangular bearing with cross-sectional dimensions of
 541 450 mm \times 650 mm, a circular bearing with diameter 600 mm, and an annular bearing with outer
 542 diameter 600 mm and inner diameter 120 mm. All the cases consist of 33 rubber layers with a
 543 thickness $t_e = 6$ mm, interspersed by 32 fiber reinforcement layers with a thickness t_f of 0.5 mm.
 544 It is assumed that the rubber has a shear modulus $G = 0.4$ MPa and a bulk modulus $K = 2000$
 545 MPa. The buckling loads presented account for the amplification due to the h/t_r ratio.

546 DATA AVAILABILITY STATEMENT

547 All data, models, and code generated that support the findings of this study are available from the
 548 corresponding author upon reasonable request.

549 References

550 Cowper, G. R. (1966). "The shear coefficient in Timoshenko's beam theory." *Journal of Applied*
 551 *Mechanics*, 33(2), 335–340.

552 Dikaros, I. C. and Sapountzakis, E. J. (2014). “Generalized warping analysis of composite beams of
553 an arbitrary cross section by BEM. I: Theoretical considerations and numerical implementation.”
554 *Journal of Engineering Mechanics*, 140(9), 04014062.

555 El Fatmi, R. (2007). “Non-uniform warping including the effects of torsion and shear forces. Part
556 I: A general beam theory.” *International Journal of Solids and Structures*, 44(18), 5912–5929.

557 Genoese, A., Genoese, A., Bilotta, A., and Garcea, G. (2013). “A mixed beam model with non-
558 uniform warpings derived from the Saint Venant rod.” *Computers & Structures*, 121, 87–98.

559 Gent, A. N. (1964). “Elastic stability of rubber compression springs.” *Journal of Mechanical En-
560 gineering Science*, 6(4), 318–326.

561 Gent, A. N. and Lindley, P. B. (1959). “The compression of bonded rubber blocks.” *Proceedings
562 of the Institution of Mechanical Engineers*, 173(1), 111–122.

563 Gent, A. N. and Meinecke, E. A. (1970). “Compression, bending, and shear of bonded rubber
564 blocks.” *Polymer Engineering & Science*, 10(1), 48–53.

565 Ghorbi, E. and Toopchi-Nezhad, H. (2023). “Annular fiber-reinforced elastomeric bearings for
566 seismic isolation of lightweight structures.” *Soil Dynamics and Earthquake Engineering*, 166,
567 107764.

568 Haringx, J. A. (1949). “On highly compressible helical springs and rubber rods, and their ap-
569 plication for vibration-free mountings, III.” *Report No. Philips Res. Rep. 4*, Philips Research
570 Laboratories, Eindhoven, Netherlands.

571 Hexagon AB (2021a). *Marc 2021.4 Volume A: Theory and User Information*.

572 Hexagon AB (2021b). *Marc 2021.4 Volume B: Element Library*.

573 Kelly, J. M. (1994). “The influence of plate flexibility on the buckling load of elastomeric isolators.”
574 *Report No. UCB/EERC-94/03*, Earthquake Engineering Research Center, Berkeley, California.

575 Kelly, J. M. (1999). “Analysis of fiber-reinforced elastomeric isolators.” *Journal of Seismology and
576 Earthquake Engineering*, 2(1), 19–34.

577 Kelly, J. M. and Konstantinidis, D. (2011). *Mechanics of Rubber Bearings for Seismic and Vibra-
578 tion Isolation*. John Wiley & Sons Ltd.

579 Lewiński, T. and Czarnecki, S. (2021). “On incorporating warping effects due to transverse shear
580 and torsion into the theories of straight elastic bars.” *Acta Mechanica*, 232, 247–282.

581 Love, A. E. H. (1944). *A Treatise on the Mathematical Theory of Elasticity*. Dover Publications,
582 New York, 4 edition.

583 Osgooei, P. M., Van Engelen, N. C., Konstantinidis, D., and Tait, M. J. (2015). “Experimental and
584 finite element study on the lateral response of modified rectangular fiber-reinforced elastomeric
585 isolators (MR-FREIs).” *Engineering Structures*, 85, 293–303.

586 Papoulia, K.-D. and Kelly, J. M. (1996). “Compression of bonded blocks of soft elastic material:
587 Variational solution.” *Journal of Engineering Mechanics*, 122(2), 163–170.

588 Pinarbasi, S. and Mengi, Y. (2008). “Elastic layers bonded to flexible reinforcements.” *International
589 Journal of Solids and Structures*, 45(3), 794–820.

590 Pinarbasi, S. and Mengi, Y. (2017). “Analysis of fiber-reinforced elastomeric isolators under pure
591 "warping".” *Structural Engineering and Mechanics*, 61(1), 31–47.

592 Simo, J. C. (1982). “A consistent formulation of nonlinear theories of elastic beams and plates.”
593 *Report No. UCB/SESM-82/06*, University of California, Berkeley, Berkeley, California.

594 Simo, J. C., Taylor, R. L., and Pister, K. S. (1985). “Variational and projection methods for the vol-
595 ume constraint in finite deformation elasto-plasticity.” *Computer Methods in Applied Mechanics
596 and Engineering*, 51(1), 177–208.

597 Steigmann, D. J. (2017). *Finite Elasticity Theory*. Oxford University Press.

598 Treloar, L. R. G. (2005). *The Physics of Rubber Elasticity*. Oxford University Press, 3 edition.

599 Tsai, H.-C. and Kelly, J. M. (2005a). “Buckling load of seismic isolators affected by flexibility of
600 reinforcement.” *International Journal of Solids and Structures*, 42(1), 255–269.

601 Tsai, H.-C. and Kelly, J. M. (2005b). “Buckling of short beams with warping effect included.”
602 *International Journal of Solids and Structures*, 42(1), 239–253.

603 Van Engelen, N. C. (2019). “Fiber-reinforced elastomeric isolators: A review.” *Soil Dynamics and
604 Earthquake Engineering*, 125, 105621.

605 Van Engelen, N. C., Osgooei, P. M., Tait, M. J., and Konstantinidis, D. (2014). “Experimental

606 and finite element study on the compression properties of modified rectangular fiber-reinforced
607 elastomeric isolators (MR-FREIs).” *Engineering Structures*, 74, 52–64.

608 Van Engelen, N. C., Tait, M. J., and Konstantinidis, D. (2016). “Development of design code
609 oriented formulas for elastomeric bearings including bulk compressibility and reinforcement
610 extensibility.” *Journal of Engineering Mechanics*, 142(6), 04016024.

Table 1. Parameters used for buckling analysis

Parameter	Value
S	10.0, 12.5, 15.0, 17.5, 20.0
S_2^*	2.0, 2.5, 3.0, 3.5, 4.0
ρ^a	0.5, 1.0, 2.0
η^b	0.0, 0.1, 0.2

^a Only applicable for isolators with rectangular cross section
^b Only applicable for isolators with circular or annular cross section

Table 2. Effective rigidities, warping properties and buckling loads for three example isolators

Parameter	Rectangular isolator	Circular isolator	Annular isolator
b (mm)	225	300	300
ρ	0.69	-	-
η	-	0.00	0.20
A (mm ²)	292,500	282,743	271,434
h (mm)	214	214	214
t_e (mm)	6	6	6
t_r (mm)	198	198	198
t_f (mm)	0.5	0.5	0.5
S	22.2	25	20
β	1.84	2.45	2.45
\widetilde{EA} (kN)	202,951	214,863	128,766
\widetilde{EI} (kN-m ²)	1,381	2,327	2,148
ω	-0.221	-0.256	-0.116
\widetilde{EJ} (kN-m ²)	5.21	8.67	55.29
B (mm ²)	68,023	59,239	61,523
C (mm ²)	56,444	38,378	52,872
f_B (mm ²)	25,090	23,067	42,301
f_C (mm ²)	3,885	18,569	34,949
P_{cr} [Eq. (6)] (kN)	3,553	4,916	2,749
P_{cr} [Eq. (9)] (kN)	3,713	4,876	2,770

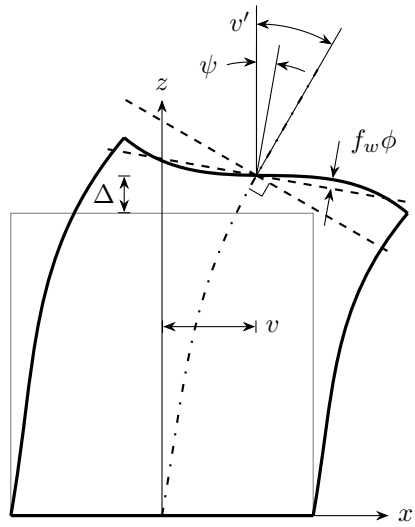


Figure 1. Generalized displacements of the beam

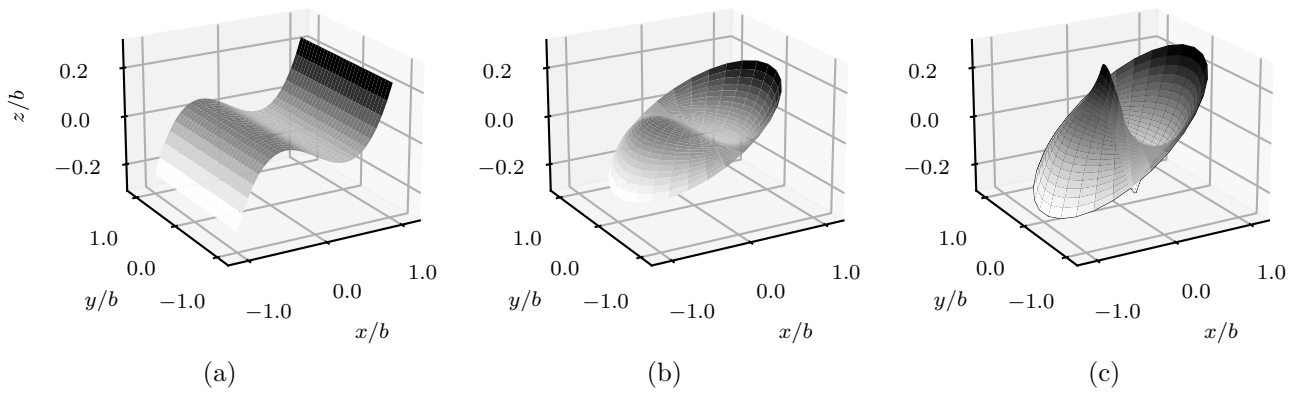


Figure 2. Warping functions for $K/G = 5000$ for (a) square cross section, (b) circular cross section, and (c) annular cross section with $\eta = 0.20$

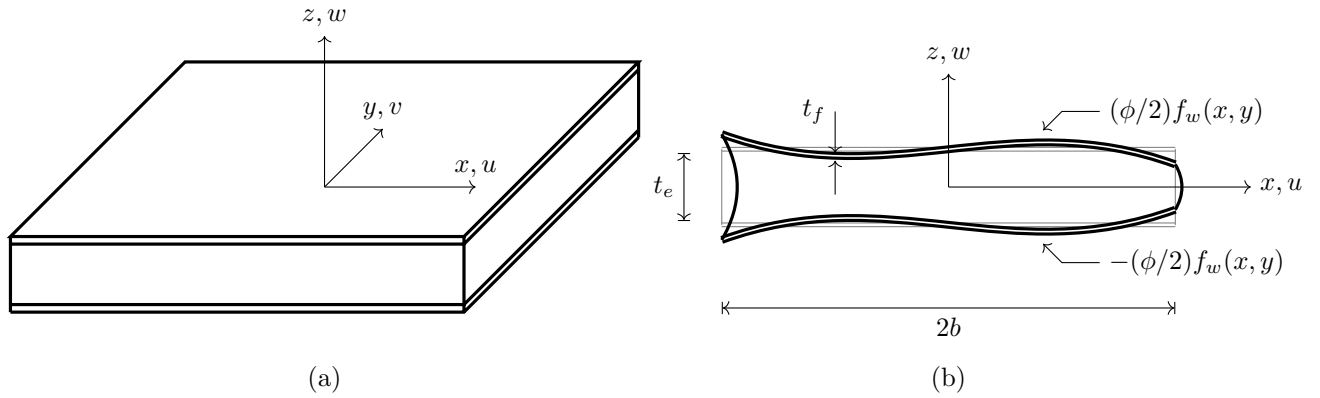


Figure 3. (a) Coordinate system for rubber layer, and (b) warping deformation of rubber layer at $y = 0$

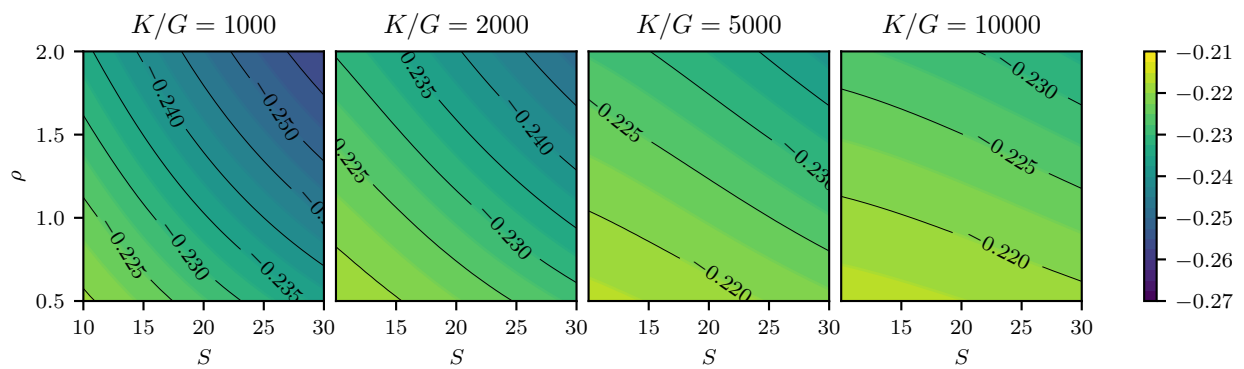


Figure 4. Numerical solution of ω for rectangular cross section

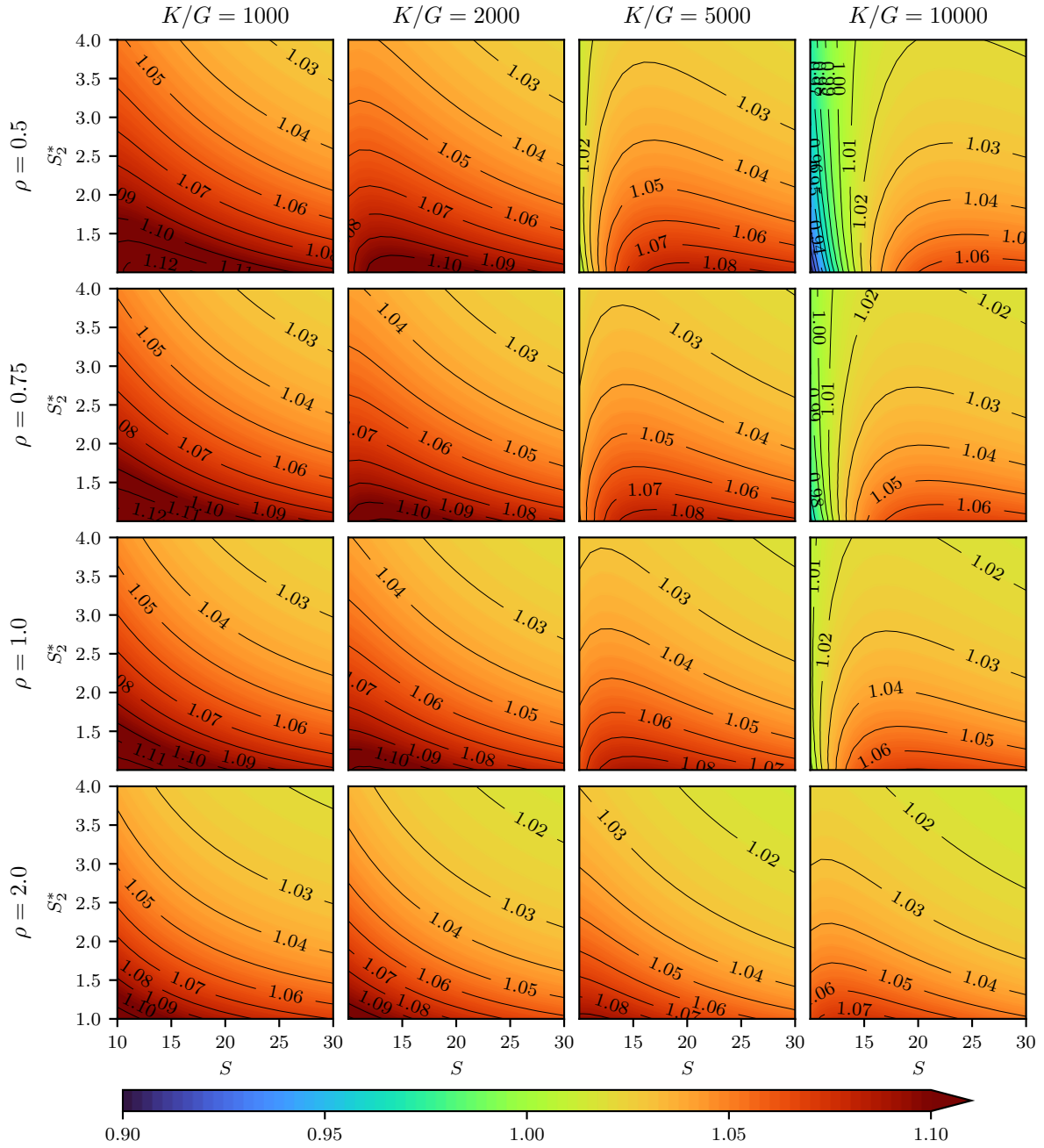


Figure 5. Ratio of P_{cr} from Eq. (9) to P_{cr} from Eq. (6) for rectangular isolators

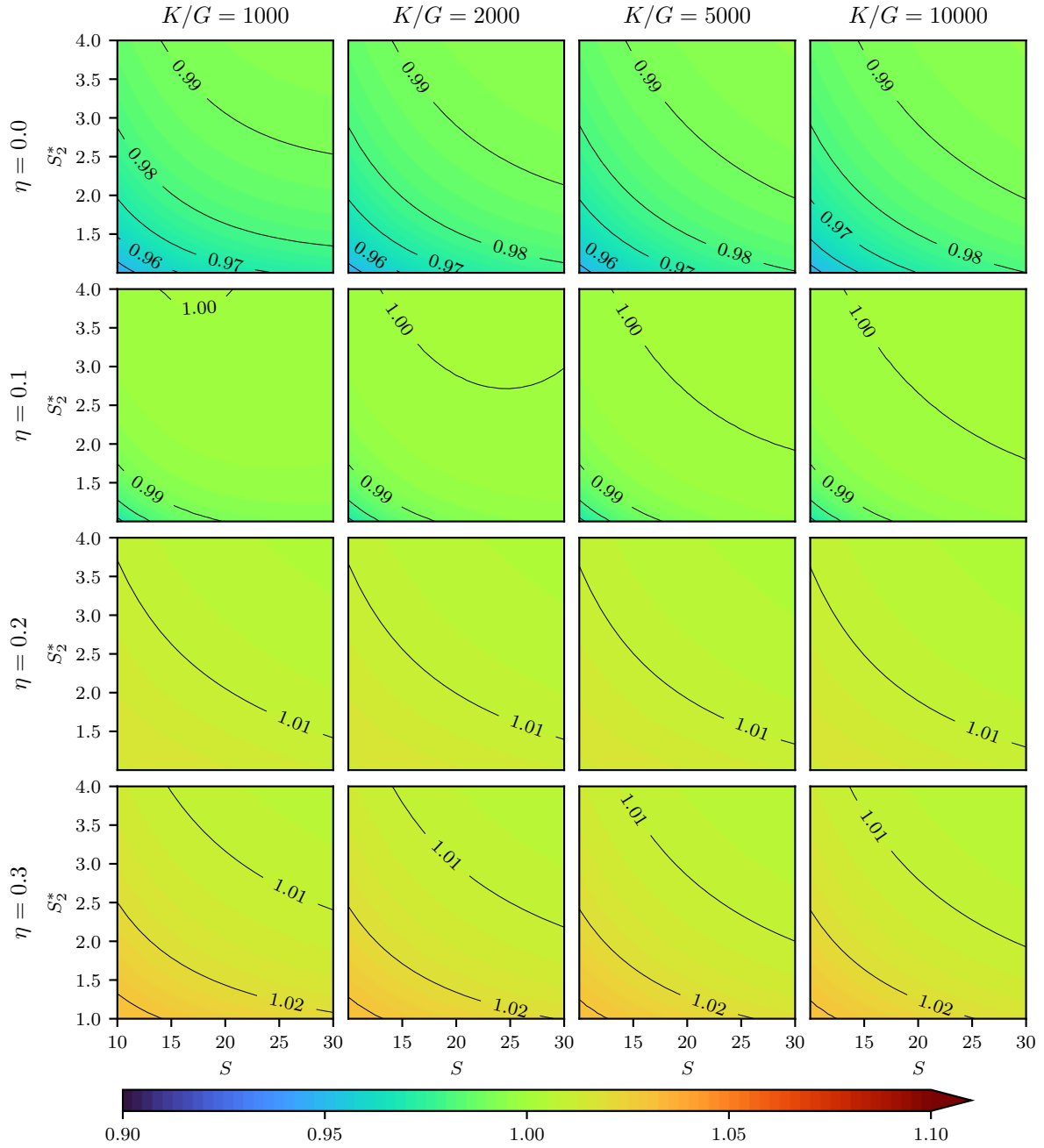


Figure 6. Ratio of P_{cr} from Eq. (9) to P_{cr} from Eq. (6) for circular ($\eta = 0$) and annular ($\eta > 0$) isolators

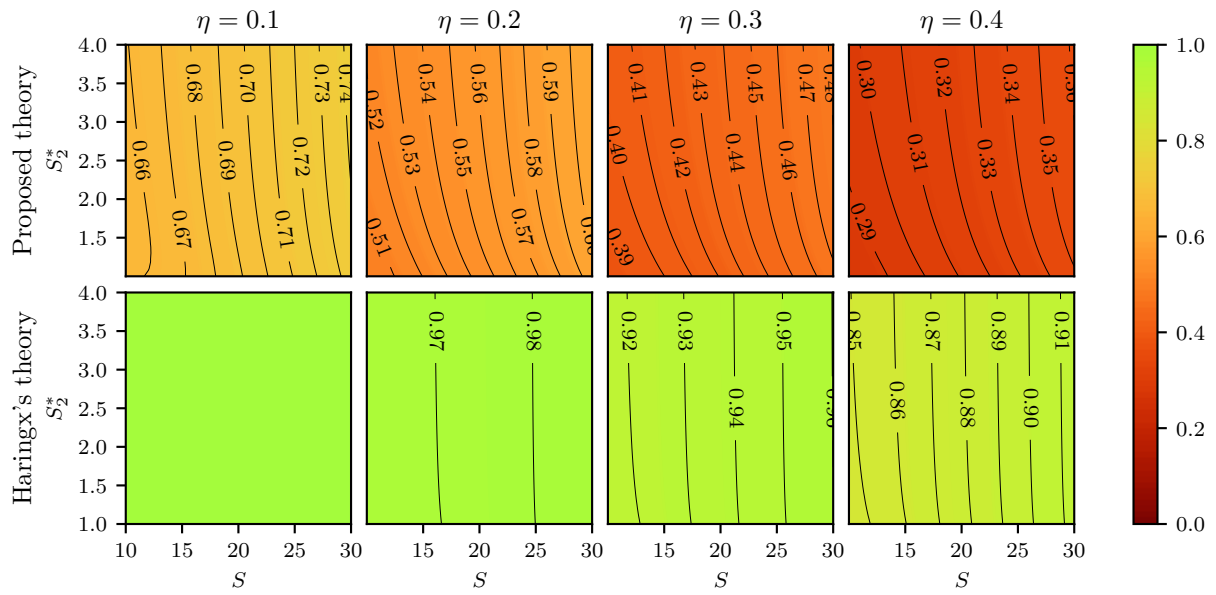


Figure 7. Ratio $p_{cr}^{\text{annular}} / p_{cr}^{\text{circular}}$ for isolators with same b and t_e for $K/G = 5000$

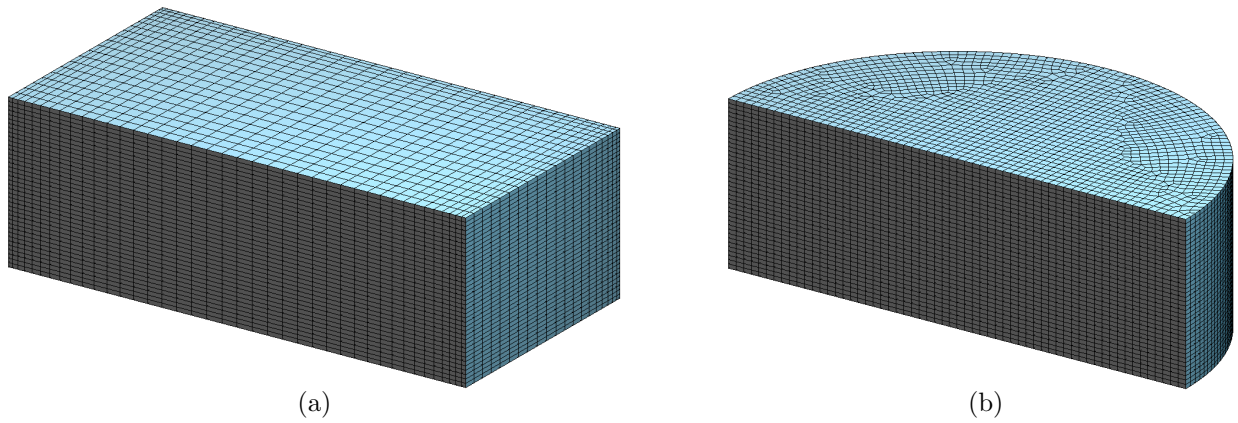


Figure 8. Mesh for (a) square and (b) circular isolator with $b = 100$ mm, $h = 100$ mm, and $S = 10$

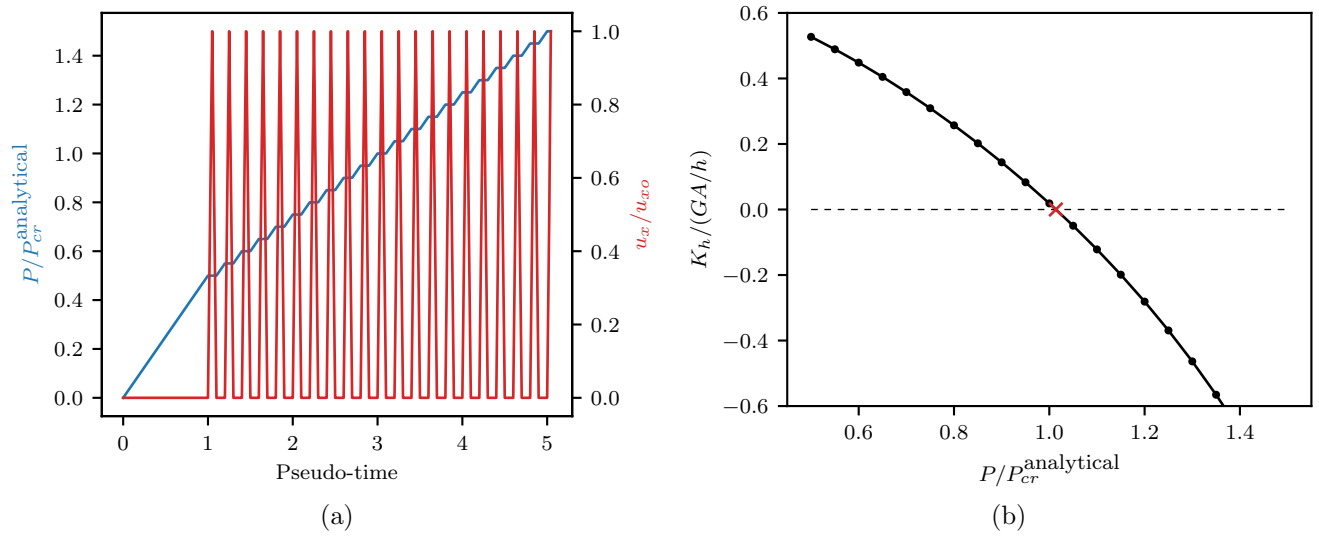


Figure 9. Method applied for estimating the buckling load in the finite element models: (a) loading protocol, and (b) estimation of critical load based on vanishing horizontal stiffness.

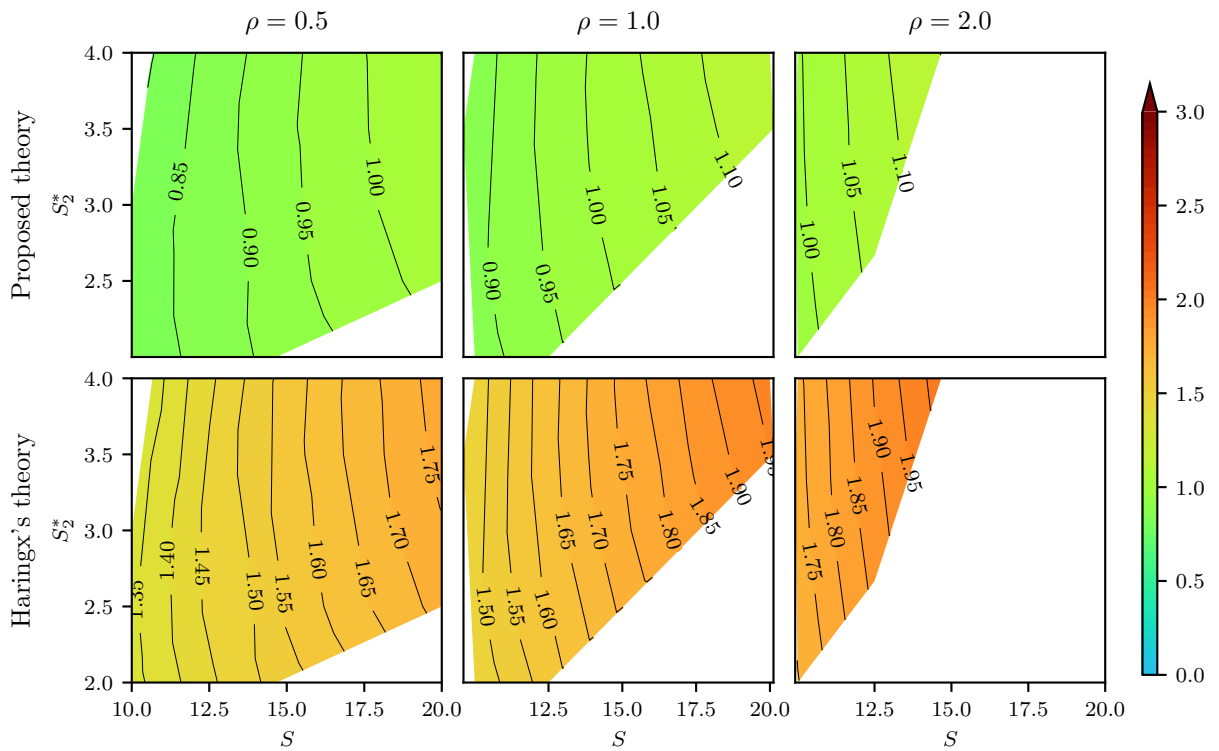


Figure 10. Ratio $P_{cr}^{analytical}/P_{cr}^{FEA}$ for rectangular isolators

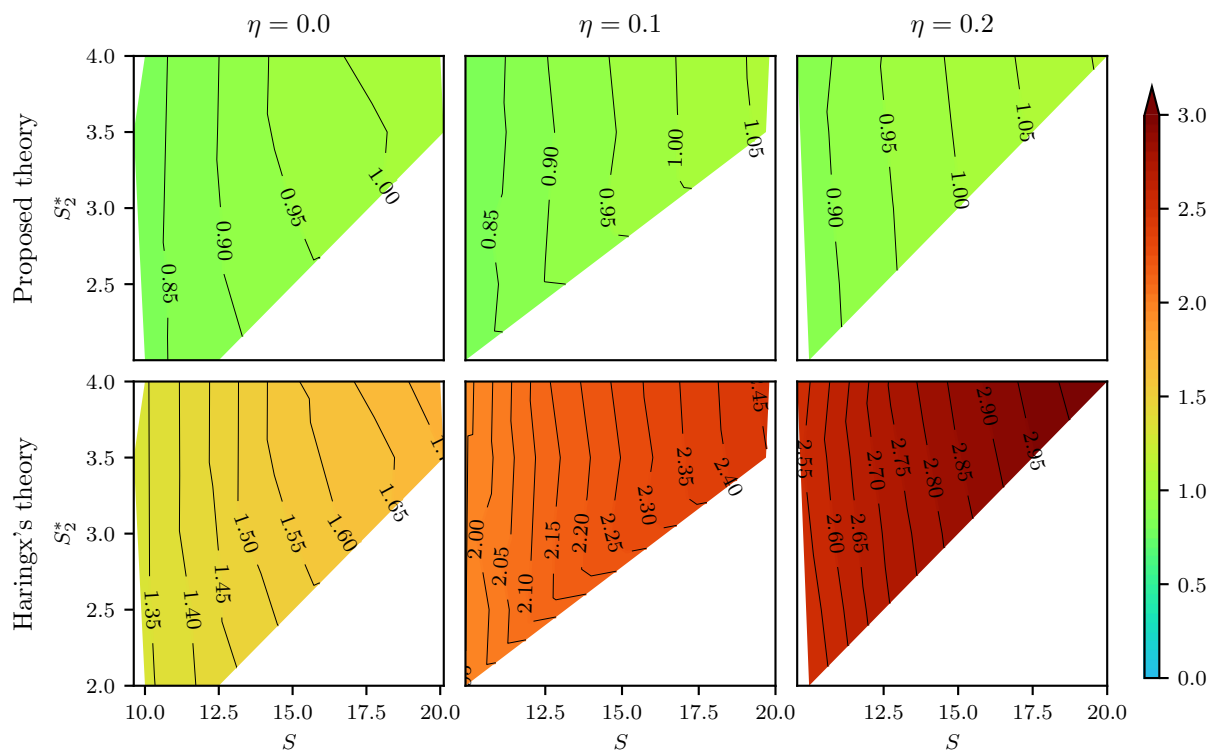


Figure 11. Ratio $P_{cr}^{\text{analytical}}/P_{cr}^{\text{FEA}}$ for circular ($\eta = 0$) and annular ($\eta > 0$) isolators

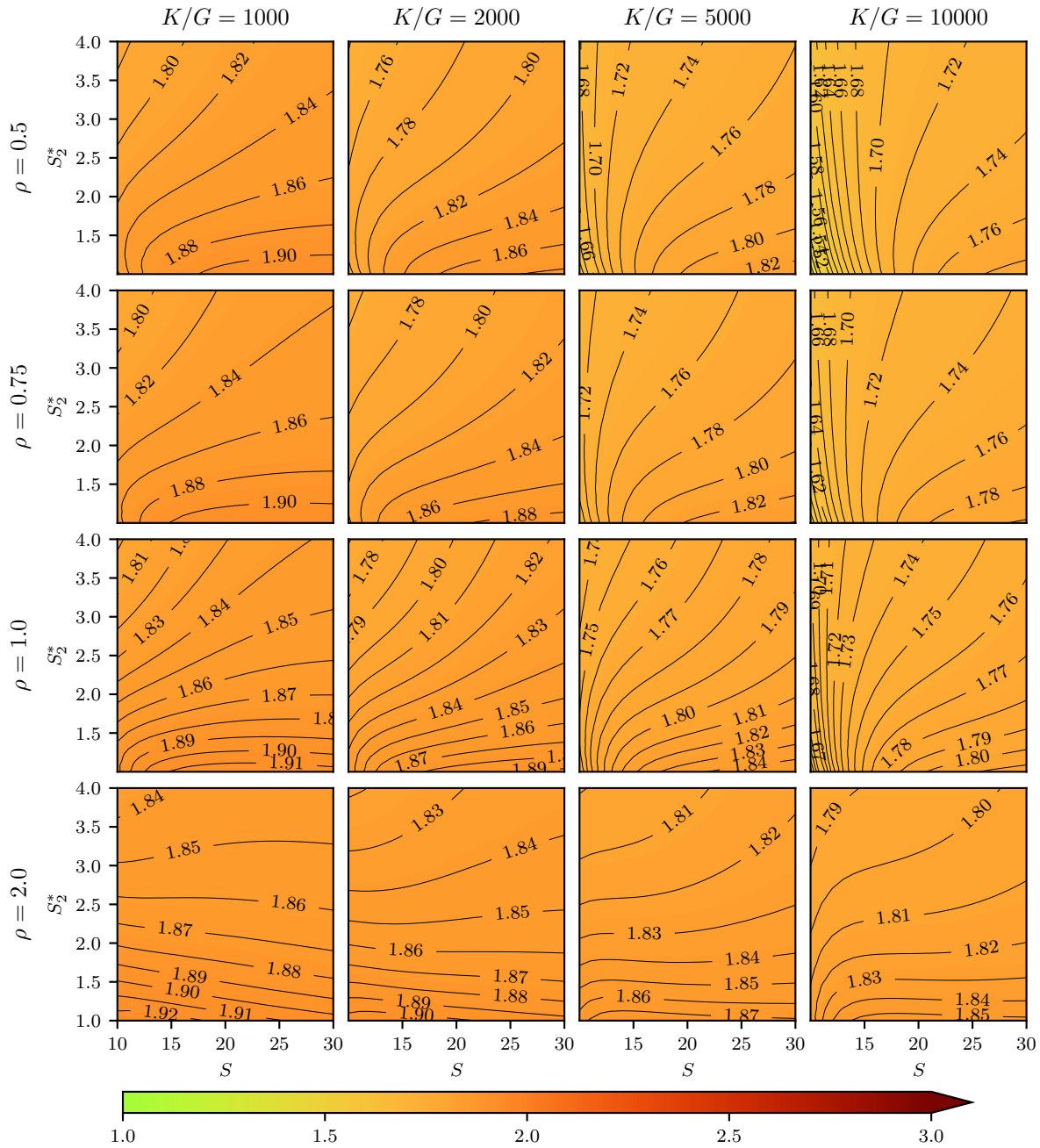


Figure 12. Reduction factor f_R for rectangular isolators

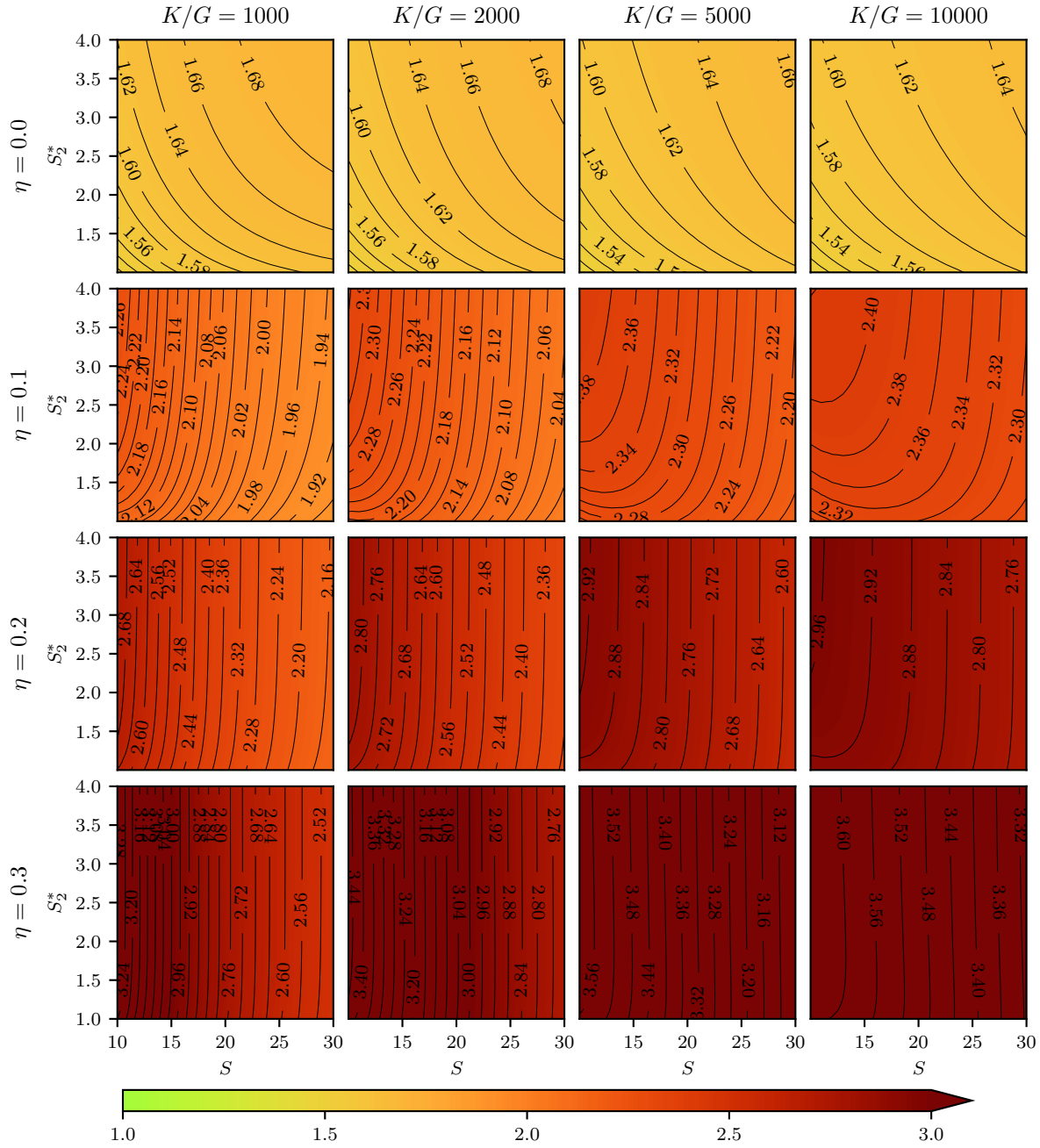


Figure 13. Reduction factor f_R for circular ($\eta = 0$) and annular ($\eta > 0$) isolators